Quenching Rate Constants and Product Assignments for Reactions of Xe(7p[3/2] 2 , 7p[5/2] 2 , and 6p'[3/2] 2) Atoms with Rare Gases, CO, H 2 , N 2 O, CH 4 , and Halogen-Containing...

ARTICLE *in* THE JOURNAL OF PHYSICAL CHEMISTRY · APRIL 1996

Impact Factor: 2.78 · DOI: 10.1021/jp952402c

2 AUTHORS, INCLUDING:

Vadim A. Alekseev
Saint Petersburg State University
61 PUBLICATIONS **211** CITATIONS

Article

Quenching Rate Constants and Product Assignments for Reactions of Xe(7p[3/2], 7p[5/2], and 6p'[3/2]) Atoms with Rare Gases, CO, H, NO, CH, and Halogen-Containing Molecules

V. Alekseev, and D. W. Setser

J. Phys. Chem., **1996**, 100 (14), 5766-5780• DOI: 10.1021/jp952402c • Publication Date (Web): 04 April 1996

Quenching Rate Constants and Product Assignments for Reactions of Xe(7p[3/2]$_2$, 7p[5/2]$_2$, and 6p′[3/2]$_2$) Atoms with Rare Gases, CO, H_2, N_2O, CH_4, and Halogen-Containing Molecules

V. Alekseev[†] **and D. W. Setser***

Department of Chemistry, Kansas State University, Manhattan, Kansas 66506

Received: August 11, 1995; In Final Form: January 16, 1996[⊗]

Two-photon excitation of Xe atoms in a static gas cell was used to prepare the Xe(7p[3/2]$_2$, 7p[5/2]$_2$, and 6p′[3/2]$_2$) states in mixtures of Xe with rare gases, H_2(D_2), CO, Cl_2, HCl, CCl_2F_2, CCl_4, SF_6, NF_3, CF_4, CH_4, CH_3F, and N_2O at 300 K. The total quenching rate constants were measured, and product fluorescence spectra were used to assign reaction pathways. The total quenching constants for these Xe* Rydberg states by molecular reagents are very large, corresponding to cross sections of 200−1500 Å^2. Qualitative models are introduced to discuss the quenching processes, which are mainly reactive quenching and excitation transfer. For reagents with very large electron affinities, ion-pair formation may be important. A correlation of the quenching cross section with the dipole moment of the reagent was observed. These three Xe* states have nearly the same energy (∼11 eV), but the Xe(7p) states nominally have the $Xe^+(^2P_{3/2})$ ion-core, whereas the Xe(6p′) states have the $Xe^+(^2P_{1/2})$ core. The XeCl(D) and XeF(D) states also have the $Xe^+(^2P_{1/2})$ core, and the fraction of XeCl(D) and XeF(D), relative to XeCl(B,C) or XeF(B,C), formed by the reactions of Xe(6p′[3/2]$_2$) atoms with halogen-containing reagents can be used to measure the degree of conservation of the $Xe^+(^2P_{1/2})$ core. The Xe(7p) and Xe(6p′) reactions actually gave nearly the same B and D distributions, with XeCl(B) and XeF(B) being favored, and the $Xe^+(^2P_{1/2})$ ion-core state is not conserved during the reactions of Xe(6p′) atoms. Two-photon excitation of the Xe(7p,6p′) states leads to intense amplified spontaneous emission (ASE) unless special feature are incorporated into the experimental design. This ASE emission can cause complications because other Xe* states are generated during the laser pulse. The measurements reported here are free from ASE, but some consequences of ASE for experiments with Xe(6p′ and 7p) excitation are summarized. The relative two-photon cross sections of the Xe(6p, 6p′, 7p) states also are discussed.

Introduction

Two-photon excitation of Xe has been used extensively to characterize the collisional relaxation of the $J = 0$ and 2 states of the Xe(6p) manifold[1−5] in rare gases and their reactions with diatomic and polyatomic reagents.[6] Less information exists about states in the Xe(6p′) and Xe(7p) manifolds,[7,8] although Keto and co-workers systematically studied the reactions of these states with Cl_2 and our laboratory made a comparison of selected Xe(6p) and Xe(6p′) states reacting with F_2, Cl_2, HCl, and CF_2Cl_2. The main point of our work was to examine the role of the $Xe^+(^2P_{1/2})$ and $Xe^+(^2P_{3/2})$ ion-cores that are associated with the Xe(6p′) and Xe(6p) states, respectively.[7] In reactions with halogen-containing molecules, Xe* states with the $Xe^+(^2P_{1/2})$ core correlate to the XeX(D) product, whereas states with the $Xe^+(^2P_{3/2})$ core correlate to XeX(B,C); X = halogen atom.[9,10] The degree of conservation of the $Xe^+(^2P_{1/2})$ core in reactions of Xe(6p′) atoms, as deduced by the ratio of XeX(D) to XeX(B), was only 10−30% depending on the reagent.[7] One ambiguity of the Xe(6p) and Xe(6p′) comparison was the ∼1 eV energy difference between these states. A more direct test for conservation of the $Xe^+(^2P_{1/2})$ core is to compare selected Xe(6p′) and Xe(7p) states, which are nearly isoenergetic (see Figure 1). The quenching rate constants and XeX(B,D) product distributions from reactions of Xe(7p[5/2]$_2$, 88 352 cm^{-1}; [3/2]$_2$, 88 687 cm^{-1}); and Xe(6p′[3/2]$_2$, 89 163 cm^{-1}) with Cl_2, HCl, CF_2Cl_2, CCl_4, and NF_3 are compared in the present study. The XeCl* and XeF* distributions from the reactions of Xe(6p), Xe(6p′), and Xe(7p) states are similar and dominated by formation of XeCl(B and C); thus, the $Xe^+(^2P_{1/2})$ core is generally not conserved in reactions of Xe(6p′) atoms. A few experiments were done with N_2O to check the branching fraction for XeO* formation.[6c,11] Experiments also were done with H_2(D_2), CO, CF_4, CH_3F, CH_4, and SF_6 to include reactants with a broad distribution of properties. The quenching rate constants for Xe(6s),[12] Xe(6p),[7] and Xe(6p′,7p) atoms illustrate the dependence of the reactivity on electronic energy. The state-resolved reactive studies of excited Na* atoms with Cl_2, O_2, and HCl,[13] the electronic-to-vibrational energy transfer reactions of Na*,[14] and the *n* and *l* changing and the ion-pair formation processes in collisions of high Rydberg states of Xe* and alkali metal atoms[15] are relevant to understanding reactions of the Xe(6p′,7p) states, which have Rydberg character.

In independent experiments with a discharge-flow reactor, we have compared the reactions of Xe(6s) and Xe(6s′) atoms with halogen-containing molecules.[16] Those experiments utilized optical pumping through the Xe(6p′ and 7p) states to transfer population from the Xe(6s[3/2]$_2$) level to the Xe(6s′[1/2]$_0$) level. As part of that effort, state-to-state rate constants were measured for several Xe(6p′,7p) states in 0.2−2 Torr of He and Ar using one-photon excitation of Xe(6s[3/2]$_2$) atoms in the flow reactor.[17] In the present work, excitation of the Xe(7p[3/2]$_2$, [5/2]$_2$, and 6p′[3/2]$_2$) atoms in added rare gas was compared to other studies of Xe(6p′ and 7p) states.[2,3] The combined data provide a comprehensive description for the state-to-state relaxation of the Xe(6p′,7p) states in He, Ar, and Ne. The state-to-state description is somewhat less complete for Kr and Xe bath gases.[3]

The experiments consist of pulsed laser excitation ($\lambda \approx 225$ nm) in a Xe/reagent mixture contained in a static gas cell. The

[†] Permanent address: St. Petersburg University, St. Petersburg, Russia.
[⊗] Abstract published in *Advance ACS Abstracts,* March 1, 1996.

0022-3654/96/20100-5766$12.00/0

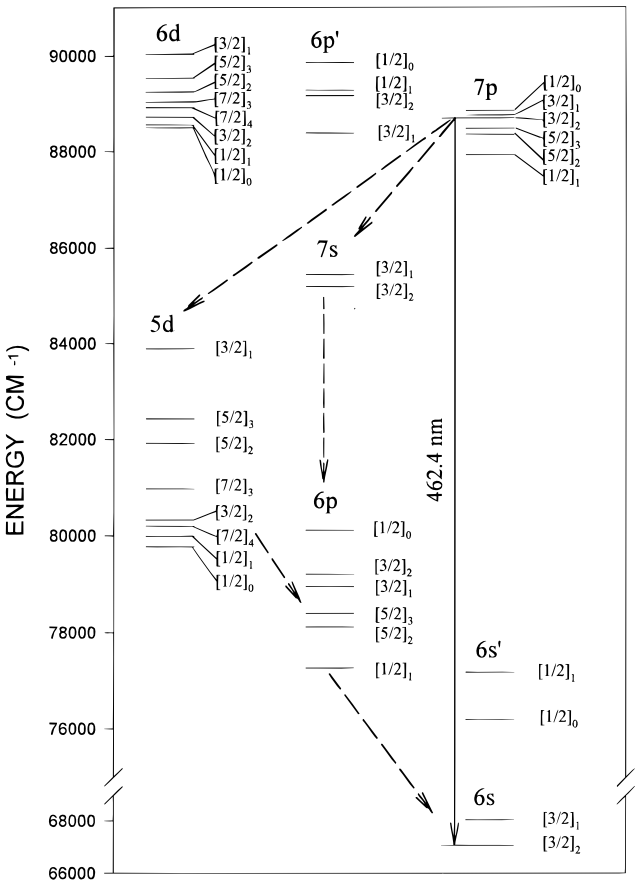

Figure 1. Energy level diagram for the excited states of xenon, which are labeled in Racah notation. The dashed and solid lines indicate the cascade and direct pathways, respectively, for ASE from Xe(7p[3/2]$_2$) to the Xe(6s) states.

rate constants were measured from the decay rate of the Xe* atomic concentration, and products were identified from fluorescence spectra. The two-photon cross sections are large, and significant concentrations of Xe(6p′,7p) atoms can be prepared with mildly focused pulses of 0.1−0.4 mJ energy. These intensities can induce nonlinear processes;[18,19] one such process is amplified spontaneous emission (ASE) from the initially produced Xe* level to several lower Xe* levels. The generation of other Xe* states during the laser pulse destroys the selectivity of the two-photon excitation, and ASE must be eliminated to study individual Xe* levels. Consequences of the ASE upon attempted kinetic measurements following Xe(6p′,7p) excitation and the design of experiments for which the ASE was eliminated are discussed.

Experimental Techniques

The Xe(6p′[3/2]$_2$, 7p[3/2]$_2$, and 7p[5/2]$_2$) atoms were prepared by two-photon absorption at 224.3, 225.5, and 226.4 nm, respectively. A Lambda Physik dye laser (LPD 3002) using Coumarin 440 dye in methanol with a BBO-I crystal and pumped by a Questek 2840 XeCl laser provided tunable UV radiation. The laser pulse had a full width at half-maximum of ∼15 ns and the energy was 0.1−0.4 mJ/pulse, as measured with a Precision power meter (Model RJP-735). The dye laser was operated without an etalon, and the band width was 22 GHz for the doubled wavelength. The Xe* and product emission spectra were observed with a monochromator (0.5 m Minuteman) equipped with an optical spectrum multichannel analyzer (OSMA, Model ST-120, Princeton Instruments) and with a Hamamatsu 955 photomultiplier tube (PMT). The output signal of the PMT was amplified (Hewlett-Packard 8447d), digitized (Hewlett-Packard 54510A oscilloscope), and transferred to a computer for storage and analysis. The spectral responses of the registration systems were calibrated with deuterium and tungsten-halogen standard lamps.

Most experiments were performed in a Pyrex glass cell that had a 1 cm distance between the entrance window (quartz flat mounted at the Brewster angle) for the laser beam and the observation zone followed by a 5 cm distance to the exit window. The short path for the laser beam was very important for avoiding nonlinear effects (see below). The laser beam passed vertically through the cell, and the entrance slit of the monochromator was parallel with the laser beam. The observation zone was viewed through a quartz window. The relative concentrations of the Xe(6p′[3/2]$_2$, 7p[3/2]$_2$, and 7p[5/2]$_2$) atoms were monitored from the intensity of the transitions to the Xe(6s) levels at 473.4, 462.4, and 469.7 nm. The quenching rate constants, the emission spectra from reactions of the isolated Xe(7p and 6p′) states, and the relative two-photon cross sections were measured in this short cell using *unfocused* laser beams. Pressures were measured by a MKS Baratron pressure transducer. Reagent gases, including Xe, were degassed and loaded into reservoirs from which the reaction cell was filled. The Xe and Kr were purchased from Cryogenic Rare Gases; other reagent gases were obtained from Matheson lecture bottles, except for CCl_4, which was obtained from a liquid sample.

The nonlinear processes and the ASE atomic emission are themselves of interest;[18,19] but, our goal was to study the reaction kinetics of Xe* states. To avoid unwanted distributions in various Xe* levels at the end of the laser pulse, the ASE must be negligible. The standard remedy is to reduce the laser pulse energy and/or to use unfocused laser radiation. This approach poses experimental problems associated with weak Xe* and reaction product emission intensities (usually 10 times weaker than for focused excitation). Due to the weak emission, we were forced mainly to use PM tubes for measurements of emission spectra, since the sensitivity of the multichannel analyzer was less than the PMT with preamplifier. Three-photon ionization and bimolecular, energy-pooling ionization of Xe* atoms[7] were of no concern for these experiments with unfocused, low-energy laser pulses.

After passing through the cell, the laser beam and associated ASE were directed to the entrance slit of a second monochromator (0.3 m McPherson) equipped with a Hamamatsu 955 PMT in order to observe the ASE; a UV filter was used to remove the laser radiation. The ASE signals, when present, were very strong even in the 850−930 nm range, where the sensitivity of the PMT is poor, and they were observed without preamplification. With the two monochromators, the Xe* emissions in the parallel and perpendicular (sideband) directions to the laser beam could be observed simultaneously. In some experiments, we used the 0.5 m monochromator to observe only the ASE by placing the cell below the slit. After passing through the cell, the laser beam was directed to the entrance slit by an additional turning prism. Some experiments to observe the ASE also were done in a conventional laser-excitation cell with 25 cm long baffle arms for the entrance and exit of the laser beam.

A summary of the ASE data will be given below. Our first experiments were done in a conventional LIF cell with a 0.5 m optical pathway between entrance and exit windows; the laser beam was focused with a 0.5 m lens. When the laser was in resonance with a 6p′ or 7p state, strong ASE in the visible region was observed in the collinear forward direction with the laser beam for either focused or unfocused conditions. The low degree of divergence of the ASE is noteworthy; the diameter

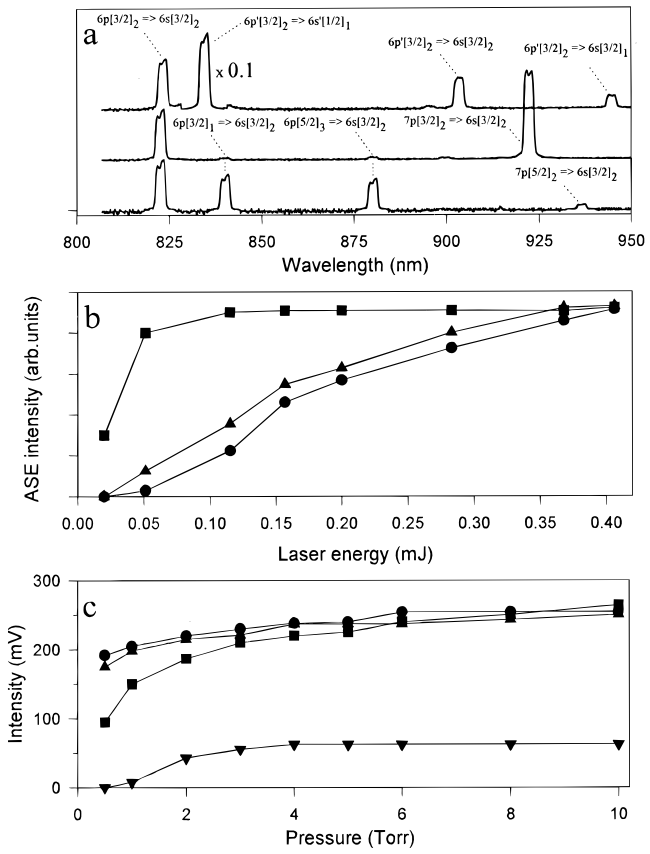

Figure 2. (a) Spectra of codirectional (ASE) emission obtained from the long cell under focused excitation from $6p'[3/2]_2$ (top), $7p[3/2]_2$ (middle), and $7p[5/2]_2$ (bottom) from 10 Torr of Xe and ~0.25 mJ pulse energy. Spectra are not corrected for the response of the OMA; the lines for $\lambda \geq 900$ nm are from the second order. (b) Intensity of codirectional emission (ASE) vs pulse energy for excitation of $6p'[3/2]_2$; the data were obtained in the long cell with 4 Torr of Xe: (■) 834.7 nm ($6p'[3/2]_2 \rightarrow 6s'[1/2]_1$) with focused excitation; (▲) 834.7 nm ($6p'[3/2]_2 \rightarrow 6s'[1/2]_1$) with unfocused excitation; (●) 823.2 nm ($6p[3/2]_2 \rightarrow 6s[3/2]_2$) with focused excitation. (c) Intensity of codirectional emission (834.7 nm line) vs Xe pressure for excitation of $6p'[3/2]_2$ for a pulse energy of ~0.2 mJ: (●) long cell with focused excitation; (■) long cell with unfocused excitation (▲) short cell with focused excitation; (▼) short cell with unfocused excitation.

of the beam was ~0.5 cm even at a distance of 1.5 m from the exit window of the cell. In addition to the visible Xe* lines, corresponding to transitions from the laser-prepared state to Xe(6s) states, the ASE spectra (Figure 2a) include some Xe(6p′−6s′) and Xe(6p−6s) transitions in the red region; the latter results from the ASE cascade via 7s or 5d states;[18] see Figure 1. The dependence of the 834.7 nm ASE transition to $6s'[1/2]_1$ following excitation of $6p'[3/2]_2$ on laser energy and Xe pressure was observed to establish the threshold conditions. This line, which is the strongest in the ASE spectrum, could be observed even for unfocused laser excitation under some conditions. The variation of the 834.7 nm intensity on laser energy for focused and unfocused conditions is shown in Figure 2b; the intensity of the 823.4 nm line from the cascade transition is shown for comparison. Unlike the cascade transition (823.4 nm line), the direct ASE transition from the laser-prepared state (834.7 nm line) is saturated for the "with lens" case at very low pulse energy. For unfocused conditions, the 834.7 nm ASE signal grows and approaches saturation at ~0.3 mJ. The 834.7 line was the only observable ASE transition for unfocused excitation of $Xe(6p'[3/2]_2)$ in these experiments.

A photolysis cell with a very short distance between the entrance and exit windows was used to avoid the ASE; Figure 2c shows the dependence of the ASE intensities from the cells with long and short arms on Xe pressure with all other conditions being the same. Some ASE was observed for excitation with unfocused radiation in the short cell, but the intensity was much weaker than for unfocused excitation in the long cell or with focused excitation in the short cell, and a well-defined threshold exists around 1 Torr (at the given laser energy and geometry of this experiment). This experiment defines the pressure and pulse energy ranges for the kinetic measurements in the short path cell, which were done in the absence of ASE.

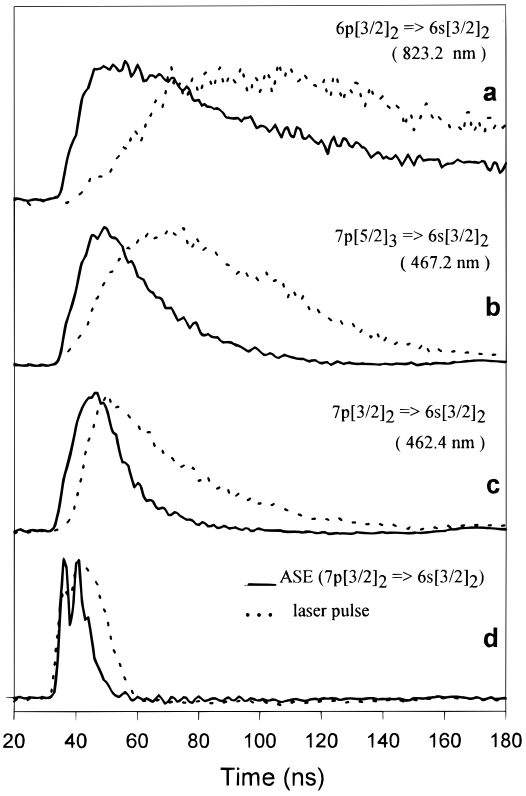

Figure 3. Waveforms of sideband emissions following excitation of $7p[3/2]_2$ in the short cell at fixed laser energy (0.25 mJ) and Xe pressure (2 Torr) for focused (solid curves) and unfocused (dashed curves) conditions. Panel (d) shows the 462.4 nm ASE emission for focused conditions and the waveform (dashed curve) of the laser pulse; experimental conditions were the same as for the sideband emission measurements.

The temporal behavior of the Xe* sideband fluorescence for focused and unfocused excitation (i.e., above and below the ASE threshold) gave some noteworthy results. In particular, the rise time of the Xe(6p → 6s) emission (Figure 3a) was much faster for focused than for unfocused excitation. The rise time of the Xe(6p) emission for unfocused excitation is determined by the rate of collision-induced transfer and *spontaneous* radiative cascade from the laser-prepared state. For focused excitation, the fast rise time is a consequence of formation of the Xe(6p) states via the *ASE* cascade transitions. The temporal behavior of the sideband emission from the 6p′ and 7p states (including the laser-prepared ones) also strongly depends on the intensity of the laser radiation. For focused excitation, the laser-excited $Xe(7p[3/2]_2)$ state has a fast, nonexponential fall time (Figure 3c) and the close-lying $7p[5/2]_3$ state has a fast rise time (Figure 3b). Experiments with the $7p[5/2]_2$ and $6p'[3/2]_2$ states gave the same results; the sideband emission from the laser-prepared state had a nonexponential fall time for focused conditions, while emission from close-lying states had faster rise times than for unfocused excitation (in particular, excitation of $Xe(6p'[3/2]_2)$ gave emission from $7p[3/2]_2$, $[5/2]_2$, and $[5/2]_3$ with fast rise

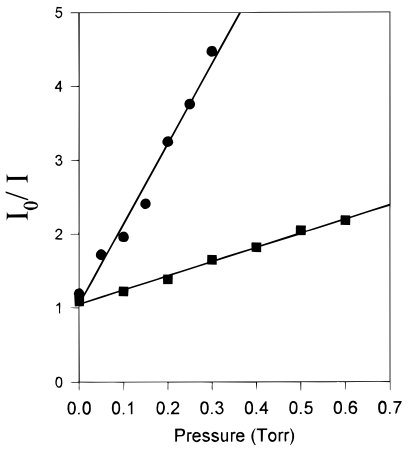

Figure 4. Plots of the ratio of the integrated intensity without Cl_2(I_0) vs the intensity with Cl_2(I) from the 462.4 nm line (see Figure 1) following excitation of Xe(7p[3/2]$_2$) for unfocused (●) and focused (■) conditions vs Cl_2 pressure.

times). Interpretation of the temporal behavior of the Xe* state concentrations for conditions that give ASE would require specially designed experiments with a shorter laser pulse. We note here that formation of the close-lying states under ASE conditions still is the result of collision-induced energy transfer from the prepared state and the fast rise time merely reflects the fast decay of the precursor state (i.e., the laser-prepared state) due to ASE. Indeed, the rise time of the Xe(7p[5/2]$_3$) emission in Figure 3b occurs within the ASE pulse; generation of a large 7p[5/2]$_3$ population after the pulse is impossible, because the Xe(7p[3/2]$_2$) laser-prepared state is depopulated during the ASE pulse. As shown in the last paragraph of this section, the "residual" concentration in the laser-prepared state after termination of the ASE pulse is 1 order of magnitude less than in the states populated by ASE. Figure 3 illustrates the extreme difficulty of studying collisional processes involving the laser-prepared Xe* state, if ASE exists.

Further demonstration that the ASE followed the laser pulse was provided by experiments in which the 462.4 nm sideband emission to Xe(6s[3/2]$_2$) was monitored following excitation of Xe(7p[3/2]$_2$) in variable pressures of Cl_2. The variation of the integrated sideband intensity vs Cl_2 pressure is shown in Figure 4. Both plots are linear, but with different slopes for the focused and unfocused experiments. Equation 1 is obtained from the equivalent of a steady-state treatment.

$$\frac{I^{o}_{Xe^*}}{I_{Xe^*}} = 1.0 + \frac{k_{Cl_2}[Cl_2]}{\tau_{eff}^{-1} + k_{Xe}[Xe]} \qquad (1)$$

The effective radiative lifetime is τ_{eff}; the other terms have their usual meaning. The $\tau_{eff}^{-1} + k_{Xe}[Xe]$ terms can be combined and defined as τ'^{-1}_{eff}, and eq 2 is obtained.

$$\frac{I^{o}_{Xe^*}}{I_{Xe^*}} = 1.0 + \tau'_{eff} k_{Cl_2}[Cl_2] \qquad (2)$$

The plots in Figure 4 give $\tau'_{eff}k_{Cl_2}$ values of 3.2×10^{-16} and 5.6×10^{-17} cm^3 for the focused and unfocused experiments, respectively. The 5.6×10^{-12} cm^3 value with $\tau_{eff} = 100$ ns and $k_{Xe^*} = 4.5 \times 10^{-10}$ cm^3 s^{-1} gives $k_{Cl_2} = (4.5 \pm 0.5) \times 10^{-10}$ cm^3 s^{-1}, which is in acceptable agreement with the measured rate constant[8a] ($(3.6 \pm 0.1) \times 10^{-9}$ cm^3 s^{-1}). Using Keto's value[8] for k_{Cl_2} and the 3.2×10^{-16} cm^3 value from Figure 4 gives $\tau_{eff} = 5 \pm 0.5$ ns for the Xe(7p[3/2]$_2$) concentration under ASE control.

In concluding this section, observations of XeCl* emission intensities are summarized from experiments with Cl_2/Xe mixtures in the short cell with pulse energies that were above and below the threshold for ASE emission. All ASE transitions from excitation of the Xe(6p′ and 7p) states eventually terminate on the long-lived Xe(6s) states. These Xe(6s) states and also the intermediate Xe(7s,5d,6p) states react with Cl_2 to give XeCl(B,C) with large branching fractions.[6−8] The relative (sideband) intensities of XeCl* and Xe(6p′,7p, or 6p) emissions can be used as a measure of the relative concentration of all Xe* states vs the concentration of the laser-excited state. Comparisons from experiments with and without Cl_2 for the same laser energy give an estimate for the fraction of directly excited atoms vs those Xe* atoms prepared via nonlinear processes. Measurements of Xe* and XeCl* emission intensities were done for pure Xe (at a pressure of 1 Torr) and for a mixture of Xe (1 Torr) with Cl_2 (1 Torr) for excitation of Xe(7p[3/2]$_2$) by focused and unfocused laser radiation (the addition of 1 Torr of Cl_2 did not remove the ASE for focused excitation). Rate constants for quenching Xe(7p[3/2]$_2$) and XeCl* by Xe and by Cl_2, which are needed for calculation of relative concentrations, were taken from previous studies[6−8] or were measured in this work; the branching fraction[2b,20] for the Xe(7p[3/2]$_2$ → 6s[3/2]$_2$) transition was used to scale the observed intensity to the total [Xe*(7p)]. Under conditions that gave ASE, the XeCl* emission intensity was ∼10 times higher than it should have been if Xe(7p[3/2]$_2$) was the only precursor to XeCl*; that is, ∼10 times as many Xe* atoms were present as Xe(7p[3/2]$_2$) atoms. On the other hand, experiments with unfocused excitation gave the *important* result that the measured [XeCl*] was equal (to within the 50% experimental uncertainty due to the low emission intensity for unfocused excitation and the difficulty of comparing atomic lines vs molecular emissions) to the expected value based on the Xe(7p[3/2]$_2$) removed by adding Cl_2. This result suggests that nonlinear processes giving Xe(7s and 5d) atoms are unimportant, and we know that Xe(6p and 6s) atoms were not generated because the ASE emission from Xe(6p) states was absent. In conclusion, experiments using unfocused laser excitation in the short cell can be used for kinetic interpretations without complications from ASE.

Experimental Results

1. Quenching Rate Constants and State-to-State Processes in Xe. Since >0.3 Torr of Xe are required for experiments with added reagent, some degree of understanding of the relaxation of the initially prepared Xe* state in Xe is needed. Although radiative lifetimes and total rate constants in Xe have been reported,[3] we decided to measure the decay constants in Xe from experiments in the short cell without focusing the laser beam, as a calibration of our experimental method. We also were able to detect weak emission from product states in the Xe(6p′ and 7p) manifolds.

The decay curves of the 6p′[3/2]$_2$, 7p[3/2]$_2$, and 7p[5/2]$_2$ states were single exponential, and the first-order decay constants are plotted vs Xe pressure in Figure 5. Two independent sets of data for the short-lived Xe(6p′) state give an intercept and slope that are in satisfactory agreement with the published work, although our reliability is ±15% because the long laser pulse limits the range of the first-order decay constant that can be measured to $\leq 5 \times 10^7$ s^{-1}. The two Xe(7p) states have established lifetimes of 100 and 120 ns.[2,3] Although our results agree with the literature to within the combined error limits, our data tend to underestimate the lifetimes; that is, the intercepts seem to be somewhat too large. Our rate constants agree very well with the experiments of Keto,[3] who used a shorter laser

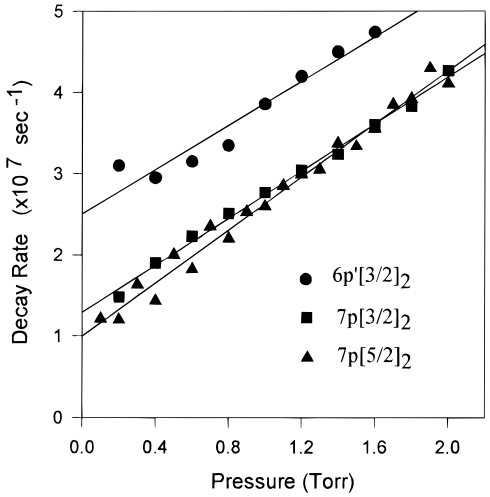

Figure 5. Stern−Volmer plots for the decay constants of $6p'[3/2]_2$, $7p[3/2]_2$, and $7p[5/2]_2$ atoms in Xe. Three independent sets of data have been merged for each of the plots. The time profiles for the laser-prepared $7p[5/2]_2$ and collisionally populated $7p[5/2]_3$ states in 2 Torr of Xe are shown in Figure 3 (dotted curves).

TABLE 1: Radiative Lifetimes and Quenching Constants of Xe($6p'[3/2]_2$, $7p[3/2]_2$, and $7p[5/2]_2$) Atoms by Xe

	τ (ns)		rate constant (10^{-10} cm^3/s)	
Xe state	this work[a]	others[b]	this work	others
$6p'[3/2]_2$	40 ± 6	35 ± 5	4.2 ± 0.5	4.3 ± 0.1[c]
	(40 ± 3)			2.6 ± 1.7[d]
$7p[3/2]_2$	100 ± 10	100 ± 10	4.5 ± 0.6	5.2 ± 0.1[c]
	(80 ± 10)			2.8 ± 0.7[d]
				2.1 ± 0.2[e]
$7p[5/2]_2$	98 ± 8	120 ± 20	5.0 ± 0.5	4.6 ± 0.1[c]
				2.8 ± 0.6[d]
				2.3 ± 0.2[e]

[a] The double entries are lifetimes from two independent sets of data; the intercepts from duplicate experiments with $Xe(7p[3/2]_2)$ seemed to have a large uncertainty even thought the slopes were always the same. [b] See ref 3a and references therein. [c] Reference 3a. [d] Reference 4a. [e] Reference 4b.

pulse and higher Xe pressures. For reasons that are not obvious, the slopes of our Stern−Volmer plots from independent data sets always were very similar, even though the intercepts showed more uncertainty. The rate constants for the two 7p levels seem to be equal, and a value of $(5.0 \pm 0.5) \times 10^{-10}$ cm^3 s^{-1} can be used as the generic rate constant for Xe(7p) states interacting with Xe; the rate constants for 6p′ levels seem to be ∼15% smaller.[3c] For Xe(7p) states with radiative lifetimes of 100−120 ns, the presence of 0.5 Torr of Xe reduces the effective lifetime by a factor of 2. The effective lifetime of $Xe(6p'[3/2]_2)$ in 0.5 Torr of Xe is only 30% shorter than the radiative lifetime.

Product fluorescence spectra from Xe(7p) states could be observed from excitation of each of the Xe(7p,6p′) levels in 1 Torr of Xe. These product intensities typically were ∼1% of the intensity from the initially prepared level, and collisional transfer among the 6p′ and 7p levels is not the major deactivation pathway. The observed lines and the assigned relative Xe* populations are summarized in Table 2. The product concentrations in Table 2 have not been corrected for quenching, so the values are lower limits to true product branching fractions. The Xe(7p) levels that are close in energy to the initially excited $7p[3/2]_2$ and $[5/2]_2$ levels account for <10−15% of the products. The waveforms in Figure 3 showed that $7p[5/2]_3$ formation develops as the $7p[3/2]_2$ level decays; that is, the two levels are not collisionally coupled. The Xe(7p) concentrations were

TABLE 2: Product Emissions[a] from Excitation of Xe($6p'[3/2]_2$, $7p[3/2]_2$, and $7p[5/2]_2$) Atoms in Xe

transition (nm)		branching fraction[b]	relative population[c] $6p'[3/2]_2$	$7p[3/2]_2$	$7p[5/2]_2$
$6p'[1/2]_0 \rightarrow 6s[3/2]_1$	458.3	0.086			
$6p'[1/2]_1 \rightarrow 6s[3/2]_1$	470.8	0.0012			
$\rightarrow 6s[3/2]_2$	450.1	0.0098			
$6p'[3/2]_2 \rightarrow 6s[3/2]_1$	473.4	0.03	1.0		
$\rightarrow 6s[3/2]_2$	452.5	0.024			
$6p'[3/2]_1 \rightarrow 6s[3/2]_1$	491.7	0.046[b]			
$\rightarrow 6s[3/2]_2$	469.1	0.014[b]			
$7p[1/2]_0 \rightarrow 6s[3/2]_1$	480.7	0.308	0.0039	0.023	
$7p[3/2]_2 \rightarrow 6s[3/2]_1$	484.4	0.056	0.0048	1.0	0.028
$\rightarrow 6s[3/2]_2$	462.4	0.373			
$7p[3/2]_1 \rightarrow 6s[3/2]_1$	483.1	0.077			
$\rightarrow 6s[3/2]_2$	461.3	0.024			
$7p[5/2]_3 \rightarrow 6s[3/2]_2$	467.2	0.387	0.0078	0.085	0.13
$7p[5/2]_2 \rightarrow 6s[3/2]_1$	492.4	0.066	0.0032	0.05	1.0
$\rightarrow 6s[3/2]_2$	469.7	0.139			
$7p[1/2]_1 \rightarrow 6s[3/2]_1$	502.9	0.0036			
$\rightarrow 6s[3/2]_2$	479.3	0.024			

[a] The data were acquired at 1 Torr Xe pressure; no adjustments have been made for quenching of the product states. [b] Taken from ref 20a. The calculated branching ratios[20a] and the experimental branching ratios[2b] differ by factors of 2 for the visible transitions for several Xe(6p′) and Xe(7p′) states. The relative intensities observed in the present work for the blue lines tend to support the data of ref 2b. The calculated fractions were used above because they are the only complete set. [c] The product populations were normalized to the laser-excited state population in each vertical column.

smaller for excitation of $Xe(6p'[3/2]_2)$ and the emission profiles were somewhat delayed, relative to those from excitation of $Xe(7p[3/2]_2$ or $[5/2]_2)$. This suggests that, at least, part of the Xe(7p) population arises from transfer through the Xe(6d) states when the $6p'[3/2]_2$ level is excited. We saw no evidence that the lowest energy $Xe(7p[1/2]_1)$ state acted as a reservoir; that is, the collisional transfer rate constants to Xe(7s and 5d) manifolds also are large.

Keto and co-workers[3c] attempted to identify products following two-photon excitation of Xe(6p′ and 7p) states. They did not observe the weak emission from Xe(6p′ or 7p) products, rather they found strong emission from the Xe(6p) levels, corresponding to rate constants that were larger than the total quenching constant. Presumably ASE existed in those experiments. Additional work is needed to identify the state-to-state rate constants for Xe(6p′,7p) with Xe. The existing data suggest a broad distribution of exit channels, including some with large energy defects. Associative ionization requires 90 000 cm^{-1}, and this channel is not open for thermal collisions of Xe(6p′,7p) atoms with ground-state Xe atoms.[21] Given the difficulty of detecting the Xe(7s,5d) states, the radiative branching[2,20] through the Xe(7s,5d) manifolds from the Xe(6p′,7p) states, and the large rate constants for most Xe* states, determination of the primary product distributions will be a challenge.

2. Quenching Rate Constants and State-to-State Processes in He and Ne. Relaxation of the Xe(7p and 6p′) states in He or Ne is known to favor product states with small ($\Delta E \approx kT$) energy defects, and collision-induced transfer back to the initially prepared state can result in multiexponential decay rates for some, but not all, states.[2,17] Unlike Xe, the magnitude of the He and Ne rate constants vary dramatically for individual Xe(6p′ or 7p) states.[2,17] Because of the long laser pulse and the effect of 0.3−0.4 Torr of Xe, we were not able to identify multiexponential components from the waveforms in He or Ne, except by indirect means. Therefore, the decay profiles in He and Ne were fitted as single exponential and the pseudo-first-order decay constants are plotted vs pressure; the *apparent*

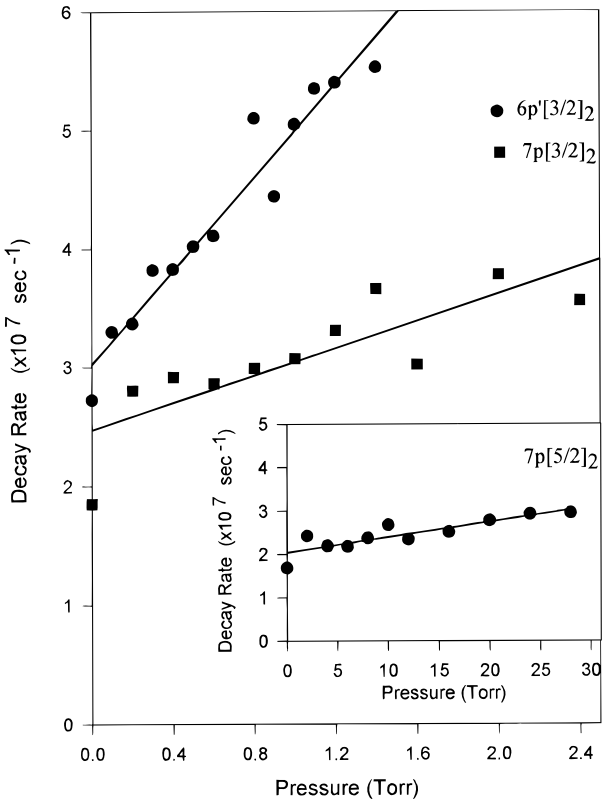

Figure 6. Stern−Volmer plots for the decay constants of 6p′[3/2]$_2$, 7p[3/2]$_2$, and 7p[5/2]$_2$ (inset) states in He. The Xe partial pressures were 0.3 Torr for 6p′[3/2]$_2$ and 7p[3/2]$_2$ and 0.4 Torr for 7p[5/2]$_2$. The He zero pressure points are not included in the fitting.

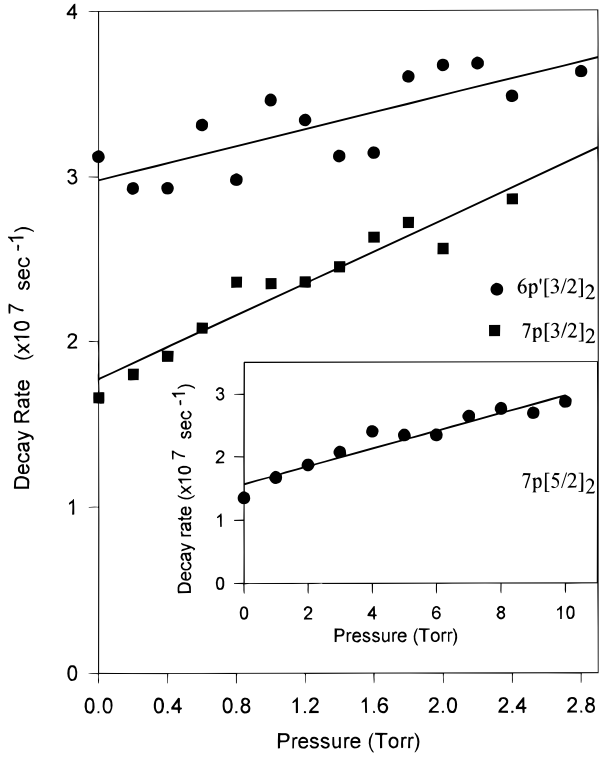

Figure 7. Stern−Volmer plots for the decay constants of 6p′[3/2]$_2$, 7p[3/2]$_2$, and 7p[5/2]$_2$ (inset) states in Ne. The Xe partial pressures were the same as described in Figure 6. The Ne zero pressure points are not included in the fitting.

second-order rate constants from linear fits to the data in Figures 6 and 7 are summarized in Table 3. The extrapolated intercepts from the He and Ne plots need not match the decay constants in 0.3 Torr of Xe, if *rapid* collisional coupling exists, because

TABLE 3: Rate Constants of the Xe(6p′[3/2]$_2$, 7p[3/2]$_2$, and 7p[5/2]$_2$) States in He and Ne

	rate constant (10^{-11} cm^3/s)		
	He	Ne	
Xe state	this work	this work	ref 2a
6p′[3/2]$_2$	57 ± 6	7.7 ± 1.5	7.0 ± 0.7[a]
7p[3/2]$_2$	13 ± 3	15 ± 2	21 ± 2[a] (∼10)[b]
7p[5/2]$_2$	1.2 ± 0.2	4.3 ± 0.3	16 ± 2[a] (∼6.4)[b]

[a] These are the total quenching rate constants reported for the specified level. [b] The values in parentheses are the slowest decay constant associated with the two-component decay for the experiments in ref 2a; hence, they are comparable to the measurements for Xe(7p) levels of this work (see text). [c] The rate constants reported here are apparent two-body constants from single-exponential fitting of the decay curves; see text for interpretation of these apparent rate constants.

the *apparent* intercept would be the effective lifetime of the coupled levels. Since one-photon excitation experiments from the Xe(6s[3/2]$_2$ state in a flow reactor with a negligible concentration of Xe have identified the relaxation mechanisms[2,17] in He and Ne, the *apparent* rate constants from Table 3 can be discussed in terms of true bimolecular state-to-state rate constants with the aid of numerically integrated rate equations describing the mechanism. One advantage of the two-photon experiments is that higher pressures can be used; the data also serve as a consistency check for interpretations of the flow reactor data.

The expected products from 6p′[3/2]$_2$ are the 6d[5/2]$_2$ and 6d[7/2]$_3$ levels, with radiative lifetimes of ∼70 ns and energy defects of −81 and +138 cm^{-1}, respectively.[17] The extrapolated intercepts of Figures 6 and 7 are consistent with the lifetime of Xe(6p′[3/2]$_2$) in 0.3 Torr of Xe; thus, the degree of collisional coupling with the 6d states is not very serious. Our rate constant in Ne, $(0.9 \pm 0.2) \times 10^{-10}$ cm^3 s^{-1}, is in modest agreement with the total quenching constant from the earlier work, 0.7×10^{-10} cm^3 s^{-1}.[2a] The apparent rate constant for He is 7 times larger than for Ne, but the value in Table 3 agrees with a recent state-to-state study ($(9 \pm 2) \times 10^{-10}$ cm^3 s^{-1}).[17] The main product in He was identified as Xe(6d[7/2]$_3$), rather than 6d[5/2]$_2$, and this is why coupled decay kinetics are not observed below ∼3 Torr of He. The state-to-state mechanism in Ne probably needs further interpretation with more attention given to 6d[7/2]$_3$ as a product.[2a] The 7p[3/2]$_1$, 7p[3/2]$_2$, and 6d[3/2]$_2$ levels, which are separated by 58 cm^{-1}, collisionally couple in He before transfer of population out of the trio of levels occurs.[17] The rate constant between 7p[3/2]$_2$ and 6d[3/2]$_2$ is especially large (18×10^{-10} cm^3 s^{-1}).[17] The radiative lifetime of 6d[3/2]$_2$ is 60 ± 5 ns, so coupling of the 7p[3/2]$_2$ and 6d[3/2]$_2$ concentrations leads to a shorter effective radiative decay rate. This is exactly what is observed in Figure 6; the radiative rate obtained by extrapolation to zero He pressure is 2.5×10^7 s^{-1}, whereas the radiative rate in 0.3 Torr of Xe is only 1.8×10^7 s^{-1}. The state-to-state experiments[17] in He gave a rate constant for the loss from the coupled levels of $(9-12) \times 10^{-11}$ cm^3 s^{-1}, and our effective rate constant (13×10^{-11} cm^3 s^{-1}) in Table 3 is for the loss of population from the coupled trio of levels. This was confirmed by inspection of the second decay component from the numerically simulated rates of these three coupled levels. On the other hand, the extrapolated intercept for Ne in Figure 6 is nearly the same as the decay rate in pure Xe, and care is needed for interpretation of the apparent rate constant. Our rate constant in Ne is somewhat larger than the decay constant assigned to the slow component following excitation of 7p[3/2]$_2$ shown in Figure 6b of ref 2a. Our *apparent* decay constant is a forced fit to both decay components and contains little new information. Although the collisional

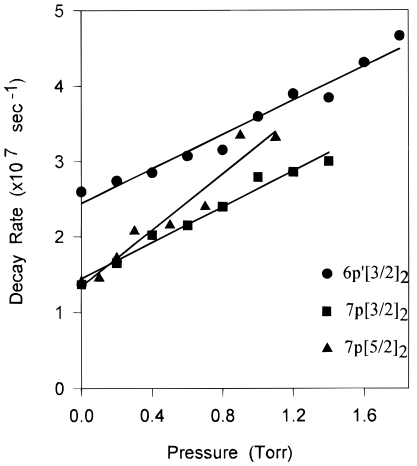

Figure 8. Stern−Volmer plots for the decay constants of 6p′[3/2]$_2$, 7p[3/2]$_2$, and 7p[5/2]$_2$ states in Kr. The Xe partial pressures were the same as described in Figure 6.

mechanisms in Ne and He are the same, the 10-fold larger coupling rate constant in He gives a much greater difference in the fast and slow decay rates.

The 7p[5/2]$_2$, 7p[5/2]$_3$, and 6p′[3/2]$_1$ levels form another coupled trio, with the radiative lifetime for 6p′[3/2]$_1$ being 2−3 times shorter than for the 7p levels; the transfer rate between the 7p[3/2]$_2$ and 6p′[3/2]$_1$ levels is the rapid step. Excitation of the lowest member, 7p[3/2]$_2$, gives pseudo-single-exponential decay, even with a 6 ns laser pulse,[2a] because τ(6p[3/2]$_1$) is shorter than for the two Xe(7p) levels. The extrapolated intercepts in He and Ne correspond to radiative rates that are slightly larger than the rates in pure Xe, because of the partial coupling to 6p′[3/2]$_1$. Our data analysis, which emphasized the pressure ranges >2 and >5 Torr for Ne and He, respectively, gave rather small apparent quenching constants. If the rate constants[2a] for transfer from 7p[3/2]$_2$ to 6p′[3/2]$_1$ and to 7p[3/2]$_3$ in Ne are subtracted from the observed k_{total}, the result matches our apparent rate constant, which is the quenching constant for the coupled trio of levels. Previous work with Ne[2a] showed that transfer to the lowest member of the 7p manifold, 7p[1/2]$_1$, was the major product from the coupled set. Spectra were recorded in 100 Torr of He following excitation of Xe(7p[5/2]$_2$), and we were able to observe emission from 7p[1/2]$_1$, which confirms this state to be the product in He. The quenching constant for 7p[1/2]$_1$ in Ne[2a] is $(0.7 \pm 0.2) \times 10^{-11}$ cm^3 s^{-1}, and the decay rate of 7p[1/2]$_1$ in our experiments suggests an even smaller value for He. The lowest levels of the Xe(7p) manifold comprise a bottleneck for the relaxation of population through the Xe(7p, 6p′, and 6d) manifolds in He and Ne. The Xe(7p[1/2]$_1$) level has a ∼150 ns[2,3] radiative lifetime, and significant Xe* concentrations can reside in the 88 000 cm^{-1} energy range for some time following excitation to the Xe*(6p′,7p,6d) manifolds in He and Ne.

3. Quenching Rate Constants for Ar and Kr. The decay profiles for the three Xe* states with added Ar and Kr were single exponential, and the first-order constants for Kr are plotted in Figure 8. Our experiments provide no new information for Ar, and the data are not shown. The six rate constants listed in Table 4 are in modest agreement with other results, although our rate constants generally tend to be larger. Previous studies[2] with shorter laser pulses also reported pseudo-single-exponential decay from these levels in Ar because the product distributions tend to be broad and the degree of reversible coupling apparently is small and hard to define. A small degree of reversible coupling between the 7p[5/2]$_2$ and 6p′[3/2]$_1$ levels probably does exist because our Stern−Volmer plot for Ar, not shown, exhibited curvature above ∼3 Torr in the same way as the data in ref 2b. Given the short lifetime for 6p′[3/2]$_2$ and the long laser pulse, our Ar rate constant in Table 4 adequately matches other results, and ∼18 × 10^{-11} cm^3 s^{-1} seems to be the best choice for the total quenching constant. The total quenching constants by Ar seem to be defined, but further work is needed to assign the primary product distributions.

TABLE 4: Rate Constants of the Xe(6p′[3/2]$_2$, 7p[3/2]$_2$, and 7p[5/2]$_2$) States in Ar and Kr

	rate constant (10^{-11} cm^3/s)			
	Ar		Kr	
Xe state	this work	others	this work	others
6p′[3/2]$_2$	25 ± 3	16 ± 2[a] 14 ± 1[b] 17.9 ± 1.4[c]	35 ± 4	29.4 ± 0.5[d]
7p[3/2]$_2$	35 ± 7	23 ± 2[a] 30 ± 3[b] 34.8 ± 3.2[c]	37 ± 5	31.1 ± 0.5[d]
7p[5/2]$_2$	30 ± 6	24 ± 2[a] 34 ± 7[b] 26 ± 2[c]	55 ± 6	40.5 ± 1.0[d]

[a] Reference 2a. [b] Reference 2b. [c] Reference 3a. [d] Reference 3c; these measurements and those for ref 3a were made with a shorter laser pulse and higher Kr pressures, thus a much greater degree of quenching.

TABLE 5: Quenching Rate Constants and Cross Sections for Xe(7p[5/2]$_2$ and 6p′[3/2]$_2$) States by Molecules

	Xe(7p[5/2]$_2$)		Xe(6p′[3/2]$_2$)	
reagent	rate constants (10^{-9} cm^3 s^{-1})	cross section[a] (Å^2)	rate constants (10^{-9} cm^3 s^{-1})	cross section[a] (Å^2)
CO	0.99 ± 0.15	190	1.4 ± 0.1	250
CF_4	0.80 ± 0.04	230	0.81 ± 0.05	240
H_2	4.5 ± 0.5	240	3.2 ± 0.4	180
D_2	3.2 ± 0.4	260	2.4 ± 0.4	190
CH_4	3.0 ± 0.5	480	1.5 ± 0.3	220
CH_3F	4.5 ± 0.3	1030	2.5 ± 0.4	520
CCl_4	3.8 ± 0.4	1300	2.3 ± 0.5	770
SF_6	4.7 ± 0.4	1550	3.4 ± 0.3	1120
HCl	3.8 ± 0.4	800	1.8 ± 0.4	380
Cl_2	3.7 ± 0.2	1000	1.9 ± 0.3	510
CCl_2F_2	2.8 ± 0.4	880	2.0 ± 0.5	630
N_2O	1.6 ± 0.2	390	1.2 ± 0.2	270
NF_3	1.2 ± 0.1	320	0.92 ± 0.08	250

[a] These are the thermal average cross sections obtained from $k(T)/\langle v \rangle$.

The rate constants for Kr given in Table 4 are, on average, slightly larger than for Ar, and they are approximately the same as for Xe; see Table 1. Emission from the Xe(7p,6p′) product levels in Kr was less than for comparable pressures of Xe. Keto[3c] reported that excitation transfer to Kr(5s and 5s′) was the major product channel from the Xe(6p′) levels, but the individual Kr* product states are not yet fully identified. As a qualitative test for excitation transfer to Kr(5s,5s′), we excited Xe(6p′[3/2]$_2$) in a mixture consisting of 0.3 Torr of Xe, 10 Torr of Kr, and 1.5 Torr of NF_3. According to the rate constants of Tables 4 and 5, the transfer to Kr* should be 2 times larger than the formation rate of XeF* from Xe(6p′[3/2]$_2$) + NF_3 for this mixture. The Kr(5s,5s′) states have long effective radiative lifetimes, and they will react with NF_3 to give KrF(B,D) or with Xe to give Xe(7s and 5d) states, which will ultimately give XeF*. The experimental results gave KrF*/XeF* ≅ 1.0, which is in good agreement with the prediction using the Kr(5s′[1/2]$_0$) rate constants for NF_3 and Xe[9]. Thus, our data support Keto's claim[3c] for transfer of energy into the Kr(5s,5s′) manifold from the Xe(6p′,7p) states rather than

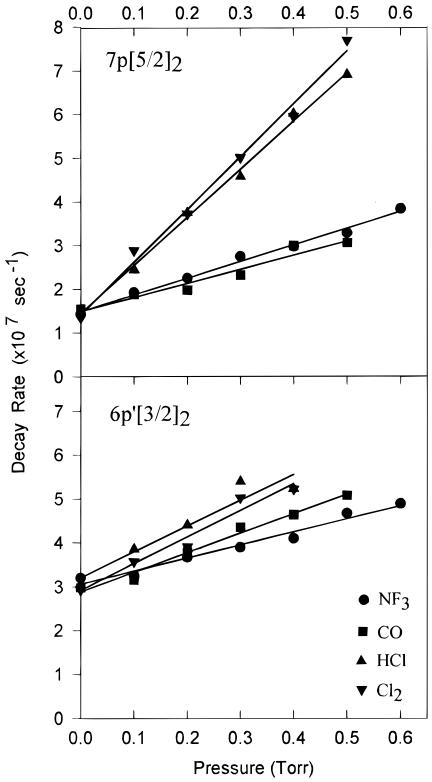

Figure 9. Stern−Volmer plots for the decay constants of 7p[5/2]$_2$ and 6p′[3/2]$_2$ atoms in NF_3, CO, HCl, and Cl_2. The Xe partial pressure was 0.3 Torr for 6p′[3/2]$_2$ and 0.4 Torr for 7p[5/2]$_2$ experiments.

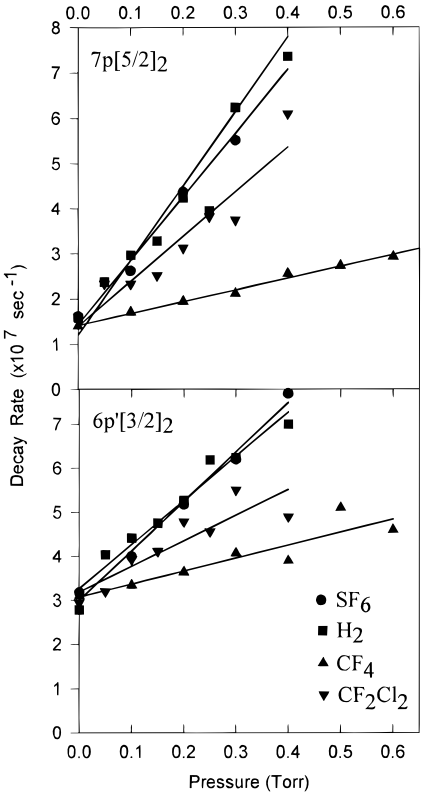

Figure 10. Stern−Volmer plots for the decay constants of 7p[5/2]$_2$ and 6p′[3/2]$_2$ atoms in SF_6, H_2, CF_4, and CCl_2F_2. The Xe partial pressures were the same as for Figure 9.

collisional redistribution within the Xe* manifold of states. Given the large number of possible (Xe−Kr)* exit channel potentials, this specificity is intriguing.

4. Quenching Rate Constants by Molecules. Pseudo-first-order decay constants were acquired for Xe(6p′[3/2]$_2$) and Xe(7p[5/2]$_2$) in 0.3 Torr of Xe with variable pressure of 13 molecular reagents to measure quenching rate constants. The experiments were done in the short cell with unfocused laser light. The waveforms were fitted as single-exponential decay rates, and the decay constants are plotted vs reagent pressure in Figures 9 and 10. The rate constants listed in Table 5 are between 0.8×10^{-9} and 4.7×10^{-9} cm^3 s^{-1}. Quenching rates of these Xe(6p′ and 7p) states by molecular reagents are very fast, and <0.6 Torr of reagent was needed to establish the Stern−Volmer plots. Preparation of the Xe/reagent mixtures with low partial pressure of the reagent and the small range of decay constants that could be measured with our long laser pulse are the limiting factors to the reliability of the constants. Most of the rate constants were measured several times in independent experiments, and the values in Table 5 were verified. A data set was accepted only if the zero reagent pressure intercept matched the sum of $\tau_{Xe^*}^{-1} + k_{Xe}[Xe]$. The large rate constants for the 7p[5/2]$_2$ state were difficult to measure because very low pressures of some reagents were needed. The SF_6 rate constant was measured several times before a reproducible result was obtained. The very large rate constant for H_2 also deserves special notice; however, the thermal cross sections for H_2 and D_2 are nearly the same, which provides confidence in the results. The rate constants for the Xe(7p) atoms tend to be larger than those for Xe(6p′) atoms for a given reagent.

The only other rate constants available for comparison are some measurements from our laboratory[6] for Xe(6p′[3/2]$_2$) with HCl (1.4×10^{-9} cm^3 s^{-1}), Cl_2 (2.1×10^{-9} cm^3 s^{-1}), and CCl_2F_2 (0.8×10^{-9} cm^3 s^{-1}) and the systematic study with Cl_2 by Keto and co-workers,[7] who found $(1.9 \pm 0.1) \times 10^{-9}$ and $(3.6 \pm 0.1) \times 10^{-9}$ for 6p′[3/2]$_2$ and 7p[5/2]$_2$, respectively. The degree of agreement is generally satisfactory. The larger k_Q(6p′) value for CCl_2F_2 in Table 5 is preferred over our earlier measurement,[6] and $k_{CF_2Cl_2}$ for Xe(6p′) is larger, not smaller, than for Xe(6p).[6] The largest cross sections are ∼1500 Å^2 for SF_6 and 1300 Å for CCl_4 with Xe(7p[5/2]$_2$), but several cross sections are >500 Å^2. Even for CF_4, H_2, and CO, the quenching cross sections are ∼200 Å^2. Checks were made for collisional transfer to other Xe(6p′ or 7p) levels with the reagents in Table 5, but no measurable emission was observed from other Xe(6p′ or 7p) levels except for CF_4, *vide infra*. Quenching by molecular reagents seems to occur by excitation transfer or by chemical reaction. Products from individual reactions are summarized below, and the quenching mechanisms are considered in the Discussion section.

5. Reactions with H_2 and CO: Searches for Products. Hydrogen was selected as a reactant, because we hoped to observe fluorescence from XeH*.[22−25] In fact, neither XeH* emission nor transfer to other Xe(6p′,7p) states was observed, and excitation transfer or chemical reaction, eq 3b, must be the mechanism.

$$\mathrm{Xe(6p'[3/2]_2) + H_2 \rightarrow XeH(B^2\Pi) + H}, \quad \Delta H_0^\circ \cong 0.13 \text{ eV} \tag{3a}$$

$$\rightarrow \mathrm{XeH(A^2\Sigma^+) + H}, \quad \Delta H_0^\circ = -0.78 \text{ eV} \tag{3b}$$

$$\mathrm{XeH^*(B^2\Pi) \rightarrow Xe + H} + h\nu \text{ (250 nm)} \tag{3c}$$

According to the observation of XeH(B) formation from $H_2(B^1\Sigma_u^+, v'=0)$ + Xe collisions,[22] reaction 3a should be endoergic by ∼0.13 eV, but possibly the true threshold energy is below the H_2(B,v'=0) state. Although formation of the

XeH(A) state should be exoergic,[25] no XeH(A−X) or XeD(A−X) emission could be detected from 400 to 830 nm. We also were unable to detect the XeH(B−X) emission at 270 nm,[22] and the threshold energy for XeH(B) formation seems to be above the $6p'[3/2]_2$ level. We believe that XeH(A) and XeD(A) must be predissociated, even though the line widths of the XeH(D−A) and XeD(D−A) emission spectra[23] do not prove predissociation, as is the case for KrH(A) and ArH(A). Formation of $H_2(B^1\Sigma_u^+,v'=0)$ is endoergic (0.13 eV), and the only excitation transfer channel is the dissociative $H_2(b^3\Sigma_u^+)$ state.

Bersohn and co-workers[26] investigated the $Xe(6p[1/2]_0) + H_2$ reaction by observing the H atoms by Lyman-α absorption. This energy is 1.1 eV lower than the $Xe(6p'[3/2]_2)$ state. If quenching occurred by (3b) followed by XeH(A) predissociation, the two H atoms should exhibit different velocities. The authors[26] found only one characteristic width for the H atom absorption profile, and (3b) seems to be eliminated. Nevertheless, the HD data are puzzling because the H/D ratio was time dependent and only reached unity after several microseconds. From the description of the experimental conditions, these experiments could have been contaminated by ASE, and reactions of $Xe(6s[3/2]_1)$ atoms may have been important.

Numerous singlet and triplet CO* product states exist at 11 eV, but we anticipated resonant excitation transfer to $CO(b^3\Sigma^+,v'=2)$, which has a 50 ns lifetime[27] for radiative decay to $CO(a^3\Pi)$ and should not be seriously quenched for pressures < 1 Torr.

$$Xe(6p'[3/2]_2) + CO \rightarrow CO(b^3\Sigma^+,v'=0) + Xe, \quad \Delta H_0^\circ = -0.54 \text{ eV} \quad (4a)$$

$$\rightarrow C + O + Xe, \quad \Delta H_0^\circ = 0.04 \text{ eV} \quad (4b)$$

$$\rightarrow CO^* + Xe \quad (4c)$$

Weak $CO(b,v'=2,1,0-a,v'')$ emission was observed for irradiation of 0.5 Torr of Xe with 2 Torr of CO for *focused* conditions, but the branching fraction for CO(b) formation was less than 0.1 (as judged by comparison to the XeCl* signal from reaction with HCl); similar results were found for experiments with $Xe(7p[5/2]_2$ and $[3/2]_2)$. Searches also were made for the $CO(B^1\Sigma^+-A^1\Pi)$ emission in the visible and $CO(A^1\Pi-X^1\Sigma^+)$ emission in the vacuum ultraviolet; emission was observed only for focused excitation. Some emission from CO(a′,d,e) was observed in the visible and red regions, but these could arise from Xe(6s,6s′) atoms formed by ASE. No emission could be observed from collisional transfer to other Xe(6p′,7p) atoms. In conclusion, the interaction of Xe(6p′,7p) atoms with CO seems *not* to be dominated by resonance excitation transfer, in contrast to the $Kr(5s'[1/2]_0$, 10.5 eV) reaction, which gives only $CO(b^3\Sigma^+,v'=0,1)$ and $CO(a'^3\Sigma^+,v'=34,35)$.[28] Quenching of Xe(6s and 6s′) atoms by CO also gives specific CO* product states, because the reactions proceed by interaction of van der Waals type entrance and exit channel potentials.[29] The much larger rate constants and the product distribution suggest that the quenching mechanism for Xe(6p′,7p) atoms by CO differs from Xe(6s′,6s) atoms.

6. Products from Reaction with N_2O and CF_4. Experiments were done with N_2O to collect XeO* emission spectra for comparison with the reactions of Xe(6p) atoms[6c] and from e-beam excitation studies of Xe/O_2 and Xe/N_2O mixtures.[30] The XeO* spectra were easily obtained, but the branching fraction for XeO* formation was only 0.1−0.2, as judged by comparison to the XeCl* emission from the HCl reaction. The XeO* spectrum, which was the same as that obtained from Xe(6p and 6s) reactions[6c,11] and is not shown, was the same as that from $Xe(6p'[3/2]_2)$ and $Xe(7p[5/2]_2)$, and the Xe^+ ion-core state does not affect the XeO* product distribution. In fact, the Xe(6p) reactions with N_2O are a preferable source of XeO* spectra, because the branching fraction seems to be higher[6c] and because the laser-scattered light for excitation of Xe(7p,6p′) obscures the principal XeO* band at 234 nm. Further work is needed to ascertain whether the 308 nm emission observed at 2 atm in e-beam excitation[30] is from the same upper state as our band at 330 nm; that is, is the latter from a vibrationally excited level? Formation of other Xe(6p′,7p) states was negligible, and the quenching mechanism seems mainly to be excitation transfer to N_2O.

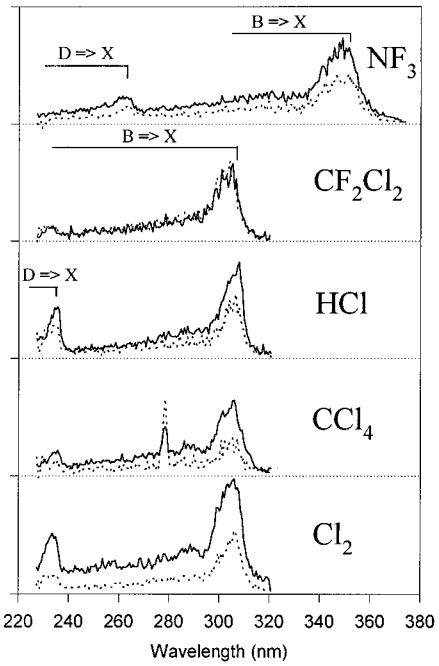

Figure 11. Comparison of XeCl(B−X) and XeCl(D−X) spectra for reactions of $Xe(6p'[3/2]_2)$ (solid line) and $Xe(7p[3/2]_2)$ (dashed line) with HCl, CCl_4, CF_2Cl_2, and Cl_2. The XeF(B−X) and XeF(D−X) spectra from NF_3 are also shown. The Xe pressures were 0.5 and 0.7 Torr and the reagent pressures were 1.0 Torr for $6p'[3/2]_2$ and $7p[3/2]_2$, respectively. All spectra were obtained for the same conditions, and the relative intensities reflect the relative branching ratios; the scans were terminated at 228 nm because of scattered laser light. The feature near 280 nm in the CCl_4 spectrum is the CCl(A−X) transition.

The quenching reaction with CF_4 generates other Xe(6p′,7p) states. For example, $Xe(7p[5/2]_2$ and $[5/2]_3)$ emission was observed following excitation of $7p[3/2]_2$, and inter- and intramultiplet relaxation constitutes a large fraction of the quenching of $7p[3/2]_2$ by CF_4. No XeF(B−X) emission was observed.

7. Products from Reactions with HCl, Cl_2, CCl_4, CF_2Cl_2, and NF_3. The XeCl* and XeF* spectra ($\lambda \geq 228$ nm) were recorded from the short cell with unfocused laser excitation from excitation of $6p'[3/2]_2$ and $7p[3/2]_2$ with 0.5 and 0.7 Torr of Xe and 1.0 Torr of reagent, respectively, for an integration time of 200 ns. The $7p[3/2]_2$ state was investigated, rather than $7p[5/2]_2$, because of the larger two-photon cross section for the former, even though the rate constants had been measured for $7p[5/2]_2$. The long-lived XeCl(C) and XeF(C) concentrations are collisionally transferred into the B states or quenched,[31] and only the D−X and B−X spectra were recorded. The spectra from HCl, Cl_2, CCl_4, CF_2Cl_2, and NF_3 are shown in Figure 11. Experiments were done for SF_6, but the XeF(B,D) yield was

TABLE 6: Relative Branching Fractions for Formation of XeCl(B,D) and XeF(B,D)[a,b]

	Cl_2	HCl	CCl_4	CCl_2F_2	NF_3
Xe* state					
6p′[3/2]$_2$	1.0	0.66	0.55	0.41	1.1
7p[3/2]$_2$	1.0	1.04[d]	0.79	1.04[d]	1.5[d]
6p[3/2]$_2$; 6p[1/2]$_0$[c]	1.0	0.70	0.65	0.14	0.60
vertical electron affinity (eV)	1.0	−0.8	0.5	≳0.0	not known
R^e_{X1} (Å)	103	7.4	22.5	≤12.6	
R^e_{X2} (Å)	10.1	4.3	7.5	≤5.9	

[a] The branching fraction for Cl_2 was assumed to be unity, and the XeCl* intensities were compared pairwise with Cl_2; see footnote *d*. The reproducibility of the branching fraction measurements was ±15%. [b] The integrated intensities were from $\lambda \geq 220$ nm. Thus, some of the XeCl* emission from the Cl_2 reaction is not included; however, the transition dipole reduces the short wavelength emission intensity, and the missing intensity is not so serious.[16] [c] These are the average values from the two highest energy Xe(6p) levels, which have energies of 80 119, and 79 213 cm^{-1}, ref 5a or ref 6d. [d] A value larger than 1.0 implies that the branching fraction for XeCl* formation from Cl_2 is less than unity; see Discussion section of text. The comparison between Cl_2 and NF_3 was repeated several times, and the result should be reliable. [e] The inner and outer crossing distances for the ion-pair and covalent potentials for Xe(7p[3/2]$_2$). The references for the EA_v are given in the text; the EA_v for CCl_4 and CCl_2F_2 are estimates.

negligible for unfocused excitation, just as for the Xe(6s,6s′)[16] and Xe(6p)[6a] atom reactions. The scans were stopped at 228 nm because of the scattered laser light. The XeCl(D−X) contribution will be slightly underestimated, but conclusions still can be made from the main bands of the B−X and D−X transitions. The differences in the spectra for the same reagent from the Xe(6p′) and Xe(7p) states are minor, but the Xe(6p′) reactions do give slightly more XeCl(D) or XeF(D) than the Xe(7p) reactions. As found previously,[7] HCl and Cl_2 exhibit the greatest yield of XeCl(D) from reactions with Xe(6p′) atoms and, hence, the larger propensity for conservation of the $Xe^+(^2P_{1/2})$ ion-core. The spectra from these Xe(6p′[3/2]$_2$) experiments without ASE are virtually the same as for the previously published spectra for the Xe(6p′) reactions.[7] Although the ASE was not directly monitored in ref 7, the role of lower energy Xe* states generated by ASE must have been minimal.[7] The apparent dependence of XeCl(D) formation on Xe pressure in the Xe(6p′) reactions with HCl that was mentioned in ref 7 probably is partly related to complications from ASE. On the basis of the low fraction of XeX(D), only a slight propensity exists to conserve the $Xe^+(^2P_{1/2})$ core by reactions of Xe(6p′) atoms.

Systematic pairwise comparisons of the XeCl(B,D−X) emission intensity from the Cl_2 reaction, relative to the other reagents, were made for constant laser energy (unfocused) to obtain *relative* branching fractions, Γ_{XeX^*}, for XeCl(B,D) and XeF(B,D) formation. The partial pressures were the same as mentioned in the above paragraph. The integrated *relative* intensities were adjusted to the same degree of quenching of the Xe(6p′) or Xe(7p) using the rate constants from Table 5. The results are tabulated as *relative* branching fractions in Table 6, assuming $\Gamma_{XeCl^*} = 1.0$ for the Cl_2 reactions. The reproducibility associated with the Γ_{XeX^*} measurements was ±15% based upon multiple experiments. We also monitored the formation of other Xe(6p′,7p) levels, but these processes were of no importance (≤1% relative to XeCl(B,D) and XeF(B,D) formation). Although Γ_{XeCl^*}(7p) for HCl and CCl_2F_2 are 1.0 to within experimental uncertainty, the $\Gamma_{XeF^*} = 1.5$ from NF_3 suggests that the assumption of unit branching for Xe(7p[3/2]$_2$) + Cl_2 is incorrect. Formation of Xe(6s[3/2]$_2$) via predissociation of XeCl* molecules formed by reaction with Cl_2 is exoergic by 0.2 eV for Xe* atoms with 11.0 eV of energy. If Xe(6s) atoms are formed, they would subsequently react with Cl_2 and contribute to the XeCl* yield. The XeCl(B,D−X) emission below 220 nm,[16] which is 10−15% of the total emission, would make the same relative contribution for both Xe(7p) and Xe(6p′) reactions. A more detailed interpretation of the product branching fractions is given in the Discussion section.

Discussion

1. Relative Two-Photon Cross Sections for Xe(6p′ and 7p) Atoms. Experiments were done to measure the *relative* two-photon cross sections for the Xe(6p′ and 7p) states for comparison with the two-photon cross sections of the Xe(6p) states. The first set of experiments were done in 7 Torr of Xe, and the relative atomic emission intensities from the excited state to the Xe(6s) states (see Table 2) were recorded for the same unfocused laser energy (∼0.3 mJ/pulse). After adjustment for radiative branching[2b,20a] and monochromator response, the relative cross sections were 1.0, 0.8, and 0.15 for the 6p′[3/2]$_2$, 7p[3/2]$_2$, and 7p[5/2]$_2$ states, respectively; the difficulty with these results is the sensitivity to the small radiative branching fractions and to the quenching constants for 7p[5/2]$_2$ and 6p′[3/2]$_2$ atoms.[2d,20] In another set of experiments, the XeCl(B−X) emission intensities from a mixture of 5 Torr of Xe, 100 Torr of He, and 1.0 Torr of Cl_2 were compared for the same pulse energy (∼0.05 mJ). With this mixture, the prepared Xe state should be deactivated to the same group of Xe* states, which then react with Cl_2 to give XeCl* without a dependence on Γ_{XeCl^*}. The high He pressure ensures transfer of XeCl(C) molecules to the XeCl(B) state. The relative cross sections for the Xe(6p′[1/2]$_0$, 6p′[3/2]$_2$, 7p[1/2]$_0$, 7p[3/2]$_2$, and 7p[5/2]$_2$) atoms were 1.2, 1.0, 0.3, 0.7, and 0.25, respectively. These experiments should be reliable because they do not involve the radiative branching ratios of the Xe(6p′ and 7p) levels or the response calibration of the monochromator. Since the absorption lines could be broadened by the 100 Torr of He, these results were confirmed for Xe(6p′[3/2]$_2$) and Xe(7p[3/2]$_2$) by comparing the XeCl(B−X) emission from excitation of 1 Torr of Xe with 1 Torr of HCl.

A set of experiments with Xe(6p) in Cl_2 were done for comparison with the Xe(6p′) data and for comparison with the Xe(6p) relative cross sections in the literature. In this case, 8 Torr of Xe and 0.2 Torr of Cl_2 were used for both the Xe(6p) and Xe(6p′) experiments. The results were confirmed by another set of comparisons with 1 Torr of Xe plus 0.5 Torr of Cl_2. Although different dyes must be used with concomitant adjustment of the laser beam, the laser pulse energies were adjusted to approximately the same value, and the comparison between the relative values for 6p vs 6p′ should be reliable to ±50%. These results gave a ratio for the two-photon cross sections for Xe(6p′[3/2]$_2$) and Xe(6p[3/2]$_2$) of unity (±50%), and the two-photon cross sections of the Xe(6p,6p′,7p) states are similar, with more difference between individual states than between the manifolds.

Many different experiments were done to establish the relative two-photon cross sections for the Xe(6p[1/2]$_0$, [3/2]$_2$, and [5/2]$_2$) states. We first measured the XeCl* emission from excitation of 1 Torr of Xe with 0.3 Torr of Cl_2 for the same unfocused laser energy (without ASE). Assuming that the Γ_{XeCl^*} are the same for these 6p states, the relative XeCl* intensity corresponds to the relative cross sections, which were 10:8:5 for 6p[1/2]$_0$, 6p[5/2]$_2$, and 6p[3/2]$_2$, respectively. The intensities of the 6p → 6s lines in the IR region were compared in the second set of experiments. This method cannot be used for the 6p[5/2]$_2$ state, because our registration system has very poor sensitivity for

the $6p[5/2]_2 \rightarrow 6s[3/2]_2$ transition (904.5 nm). We used 1 Torr of Xe and the same laser energy as for the XeCl* experiments. The intensities of $6p[1/2]_0 \rightarrow 6s[3/2]_1$ and $6p[3/2]_2 \rightarrow 6s[3/2]_2$ lines were adjusted for response of the registration system and for branching ratios to obtain relative cross sections for $6p[1/2]_0/6p[3/2]_2$ of 2:1, i.e., the same as from the experiments based on the relative XeCl* emission intensities. Our relative cross section for the $Xe(6p[3/2]_2)$ state disagrees with previous measurements.[3d,33] According to Gornik et al.,[33] who recorded the relative atomic emission intensities (presumably with filters) from very low pressure (2.6 μbar = 0.002 Torr) experiments with a mildly focused laser beam, the ratio is 9:5:1 for $6p[1/2]_0$, $6p[5/2]_2$, $6p[3/2]_2$. High-pressure (1000−2800 Torr) measurements by Keto and co-workers[3d] gave 8:4:1, based on the relative Xe_2* emission intensities. We also tried this method to check our results. Experiment were done with a Xe pressure of 300 Torr and laser energy of 0.16 mJ; the Xe_2* emission was observed in the 180 nm range with the 955 Hamamatsu PMT. To avoid absorption of the vacuum UV emission, the monochromator was purged with nitrogen. The ratio of Xe_2* emission intensities from excitation of the $6p[1/2]_0$ and $6p[3/2]_2$ states was 2:1 and 10:6 for focused and unfocused excitation, respectively, which is in good agreement with the results obtained above. The same experiment with the $6p[5/2]_2$ state gave nearly the same Xe_2* intensity as excitation of the $6p[1/2]_0$ state, which is consistent with our low-pressure results. Due to pressure broadening, the low- and high-pressure cross sections could be different, and we decided to concentrate our attention on additional low-pressure measurements to examine the discrepancy between the cross sections for $6p[1/2]_0$ and $6p[3/2]_2$. Systematic experiments (in the short cell) using the XeCl* method for laser energies of 0.03−0.5 mJ and for various Xe/Cl_2 mixture compositions always gave the 2:1 ratio, within 20% uncertainty, for $6p[1/2]_0$ vs $6p[3/2]_2$. Even focused experiments with laser energies ≤ 0.2 mJ, which does cause ASE, gave the 2:1 ratio of cross sections. The same ratio was also obtained from the Xe* atomic line intensities; unfocused excitation gave slightly smaller ratios than those obtained with the same method for focused excitation; typical ratios were 2:1 and 10:3 for focused and unfocused conditions, respectively. Despite using a variety of experimental conditions, we were unable to reproduce the previously published[3d,33] ratio (8−9) for the cross sections of $6p[1/2]_0$ to $6p[3/2]_2$ states. As a result of these extensive experiments, we believe that the ratio of two-photon cross sections for $6p[1/2]_0$ and $6p[3/2]_2$ must be 2−3 and not 8−9; all investigators agree that the cross sections for the $6p[1/2]_0$ and $6p[5/2]_2$ states are comparable.

In principle, comparison of the experimental and calculated relative two-photon cross sections would be useful. For constant laser power and bandwidth, the two-photon cross section is proportional to the *square* of the two-photon matrix element, $M_{f,g}$.

$$M_{f,g} = \frac{2\pi}{h}\sum_k \frac{\mu_{kf}\mu_{gk}}{(\omega_{gk} - \omega_L)} \qquad (5)$$

Unfortunately, the dipole matrix elements in eq 5 can be either positive or negative and the signs are usually not reported. Therefore, the sum over all relative states cannot be evaluated. We did do the summation specified in eq 5 using oscillator strengths, which is equivalent to assuming that all the matrix elements are positive, and these results are available as supporting information. The calculated relative cross sections from this assumption are in modest agreement with the experimental data. As Gornick noted, the calculated relative cross sections based on just the Xe(6s) intermediate state also would agree with our experimental results for the $6p[1/2]_0$, $6p[3/2]_2$, and $6p[5/2]_2$ states. However, the validity of these assumptions is impossible to evaluate.

The larger the two-photon cross section, the more likely the onset of ASE from a given level for the same laser power. This seems qualitatively to be the case, because ASE was stronger for excitation of the 6p′ states than the 7p states, especially the ASE from the Xe(6p′−6s′) transitions (the favorable radiative branching fractions from the 6p′ state also is a factor). In future work,[32] we will utilize the ASE from excitation of Xe(6p) and Xe(6p′) levels as a means to selectively generate and study the $Xe(6s[3/2]_1)$ and $Xe(6s'[1/2]_1)$ resonance states. Our work provides no fundamental insight into the origin of the nonlinear interactions, which we have called ASE. Rankin et al.[18a] assigned the phenomenon mainly to true resonance-amplified stimulated emission, but contributions from other nonlinear process, such as hyper-Raman, also are possible.[32]

2. Correlation of Quenching Cross Sections with Properties of Molecular Reagents. Quenching rate constants for the Xe(6p′ and 7p) states generally are 3−4 times larger than for the $Xe(6p[3/2]_2)$ state.[7] The threshold energy for associative ionization is above the Xe(6p′) energy, so ionization channels need not be considered except for ion-pair formation from reagents with EA ≥ 1 eV. Such large cross sections invite comparison to long-range quenching models. The orbiting criteria, with possible modifications, were the most useful model to correlate the cross sections for Xe(6s) atoms.[12] If the attractive part of the entrance channel potential is described by $V(r) = -C_6/r^6$, the orbiting cross section is defined by eq 6.

$$\sigma_Q(E) = P(3/2)\pi(2C_6/E)^{1/3} \qquad (6)$$

P is the probability of quenching for trajectories of translational energy, E, that pass within the orbiting distance and C_6 is the coefficient of the interaction potential between Xe* and Q. Integration over the thermal Boltzmann energy distribution gives the thermal cross section.

$$\sigma_Q(T) = P\pi(2/3)^{2/3}(2C_6/kT)^{1/3} \qquad (7)$$

The C_6 coefficients can be calculated from the Slater−Kirkwood approximation

$$C_6 = C_{\text{dip-ind.dip}} + C_{\text{dis}} = \mu Q\alpha^2_{Xe^*} + (3/2)ehm^{-1/2}\{\alpha_{Xe^*}\alpha_Q/((\alpha_{Xe^*}/N_{Xe^*})^{1/2} + (\alpha_Q/N_Q)^{1/2})\} \qquad (8)$$

e and m are the charge and mass of the electron, μ_Q is the dipole moment of Q, α is the polarizability, and N is the effective number of electrons, which is l for Xe*. The term corresponding to dipole-induced dipole interaction was small relative to C_{dis} for Xe(6s) atoms.[12] However, the polarizabilities of the Xe(6p and 7p) atoms are ∼3.3 and ∼75 times larger than for the Xe(6s) atoms,[34] and a greater dependence of $\sigma_Q(T)$ on μ_Q can be expected. A plot of ln σ_Q vs ln μ_Q is shown in Figure 12, and a correlation for Xe(6p′ and 7p) atoms does exist. The apparent goodness of the correlation may be accidental because of the small number of points (the slopes of ln σ_Q vs ln μ_Q plots for the $6p'[3/2]_2$ and $7p[5/2]_2$ states are ∼1/3 and ∼1/2, respectively, instead of the expected 2/3). Nevertheless, this correlation with μ_Q is of interest for further testing[32] with Xe* Rydberg states, since $C_{\text{dip-ind.dip}}$ depends on α_{Xe}^2, while C_{dis} depends on $\alpha_{Xe}^{1/2}$ (the $\alpha_{Xe}^{1/2}$ arises because $\alpha_{Xe^*} \gg \alpha_Q/N_Q$ for Rydberg states; see eq 8).

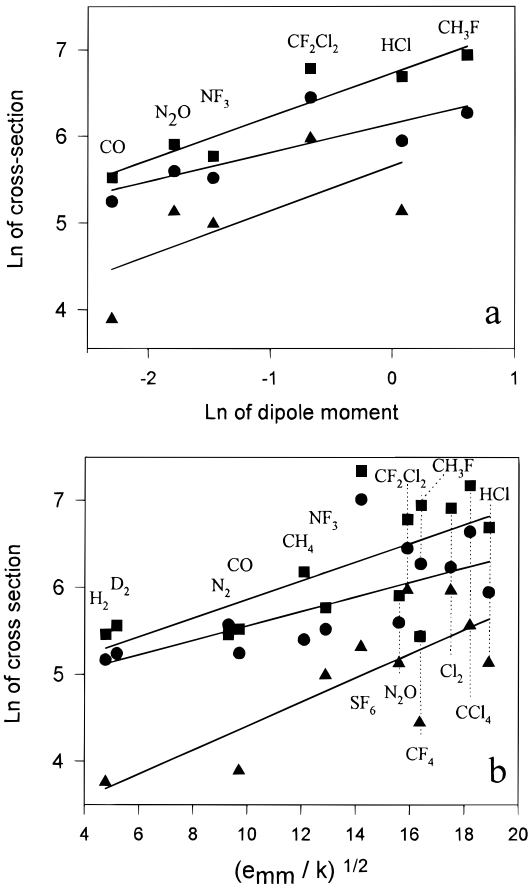

Figure 12. (a) Plots of quenching cross sections vs reagent dipole moment for the Xe(6p′[3/2]$_2$) (●), Xe(7p[5/2]$_2$) (■), and Xe(6p[3/2]$_2$) (▲) states. The data for Xe(6p) were taken from ref 7. (b) Plots of quenching cross sections vs the square root of the van der Waals well depths of the reagent for Xe(6p′[3/2]$_2$) (●), Xe(7p[5/2]$_2$) (■), and Xe(6p[3/2]$_2$) (▲).

The cross sections for the Xe(6s), Xe(6p), and Xe(7p) atoms do scale with the increased polarizability of Xe*, but not in quantitative agreement with eq 7. Since the dipole-induced-dipole term is important and since terms other than C_6 also can contribute to the long-range potential,[3d] a plot of ln $\sigma_Q(T)$ vs α_Q was not very useful. Slightly better correlations[12] were found for the Xe(6p′), Xe(7p), and Xe(6p) cross sections with the van der Waals well depth, (ϵ_Q/k);$^{1/2}$ see Figure 12; this plot is more successful because ϵ_Q takes into account dispersion and other long-range forces. The Cl_2, CCl_4, and SF_6 experimental points tend to lie above the correlation line, because of the interaction of the covalent potential with the ion-pair potential, $V(Xe^+;Q^-)$, at long range. Since the electron affinities of NF_3, HCl, and CF_2Cl_2 are smaller, the ion-pair potentials should play a lesser role in determining σ_Q. A set of rate constants for reagents with a common quenching mechanism would be preferable to the group in Table 5 for searching for correlations with physical properties of the reagent.

3. Conservation of the Xe$^+$(^{2}P$_{1/2}$) Core in Reactions of Xe(6p′[3/2]$_2$) with RX Molecules. A reaction mechanism based on the crossing of the flat covalent, V(Xe*;RX), entrance channel potential and the two ion-pair potentials, $V(Xe^+(^2P_{3/2});RX^-)$ with an outer crossing seam centered at R_{X1} and $V(Xe^+(^2P_{1/2});RX^-)$ with an inner crossing seam centered at R_{X2}, was discussed in our earlier paper.[7] The present work confirms that the Xe(6p′[3/2]$_2$) atoms mainly interact at the outer crossing, as judged by formation of XeX(B,C) rather than XeX(D). The branching fractions for XeX* formation from Xe(6p′) reactions seem to be ≥0.6, which is large enough to exclude the possibility that coupling to dissociative RX* states between R_{X1} and R_{X2} was the main cause for the low yield of XeX(D). The experimental data are unequivocal in showing that coupling at the outer crossing (or an equivalent mechanism that gives XeX(B,C)) is important for all halogen-containing reagents (SF_6 is a special case) regardless of the value of the vertical electron affinity (see Table 6). Although this is the main conclusion, the actual yield for XeX(D) does depend upon reagent, and 20−30% of the trajectories for HCl and Cl_2 do reach R_{X2}. Our experiments provide no quantitative information about the formation of XeX(C). Although some XeX(C) is formed,[7] collisional transfer to XeX(B) prevents assignment of a C/B ratio.

One explanation of why Xe(6p′) atoms + RX collisions couple to the outer ion-pair potential with apparent change of ion-core at very long range is the intrinsically mixed nature of the Xe$^+$ core for Xe(6p′) and Xe(7p) states.[35,36] For example, the purity of the Xe(6p′[3/2]$_2$) core is only 89% because of mixing with the Xe(7p[5/2]$_2$) state.[35,36] The intrinsically mixed nature of the ion-cores also explains why reactions of Xe(7p) atoms give some XeX(D). The only state with a pure core in the two manifolds is Xe(7p[5/2]$_3$) because no Xe(6p′) state with $J = 3$ exists. This mixed nature of the ion-cores also explains some of the surprisingly strong Xe(6p′−6s) and Xe(7p−6s′) radiative transitions.[20] The generally smaller rate constants for the Xe(6p′) reactions probably is a reflection of the reduced probability for coupling at R_{X1}. The arguments of these two paragraphs are based upon the covalent−ionic curve-crossing model,[8] but the same general conclusion would follow for a mechanism based on the "three-body" interaction of the reagent molecule with the Rydberg electron and the Xe$^+$ core of the Rydberg atom with the physical size and polarizability associated with $n = 6$ or 7.[15] The results for SF_6 and CCl_4 also seem consistent with the free-electron model, *vide infra*.

Sulfur hexafluoride has the largest quenching cross section in Table 5, but it gives a negligible yield of XeF*. The interaction of SF_6 with Xe*(n=25) Rydberg states has an immense cross section (∼64 000 Å^2) for ion-pair formation ($Xe^+ + SF_6^-$), and cross sections for Rydberg states of alkali metal atoms are comparable.[15g] The ion-pair formation cross sections decline for intermediate n, and the value is 1600 Å^2 for K(n=9) atoms.[15g] On the basis of these results, we believe that the quenching of Xe(6p′,7p) by SF_6 with cross sections of 1550 and 1120 Å^2 proceeds by a similar mechanism; for example, SF_6 interacts directly with the Rydberg electron. Since EA(SF_6) = 1.2 eV, ion-pair formation is only 0.1 eV exoergic and the branching fraction for ion-pair formation from 300 K collisions of Xe(7p) + SF_6 collisions is not large; that is, most of the $Xe^+;SF_6^-$ pairs will not have enough kinetic energy to escape from the Coulomb field.[37] The SF_6^- ion is bound, and the conventional explanation for the absence of XeF* from reactions of Xe(6s or 6p) atoms is that the $Xe^+;SF_6^-$ pair predissociates to the Xe;SF_6* continuum before crossing the potential barrier[39] leading to SF_5 + XeF(B,C). On the other hand, the Xe$^+$ and SF_6^- recombination reaction *does* give some XeF*.[10b,c] The entrance channel energies for $Xe^+ + SF_6^-$ and Xe(7p) + SF_6 are similar, and the apparent difference in exit channels for these two reactions is puzzling. Sulfur hexafluoride also is unique as a reactant in showing no spin−orbit effects in reactions with Ca(4p^{3}P$_J$ and 3d^{1}D) states.[38] Two SF_6^- states exist;[39] perhaps the initial state from the harpoon event is not the ground state of SF_6^-, or perhaps more information is needed about the different dissociation channels of SF_6^-.[39e] Understanding this puzzle could be aided by knowing Γ_{XeF^*} for the $Xe^+ + SF_6^-$ recombination reaction.

The assumption of $\Gamma_{XeCl^*} = 1.0$ from Xe(7p[3/2]$_2$) with Cl_2 gave $\Gamma_{XeF^*} > 1.0$ for NF_3 and slightly above unity for CF_2Cl_2 and HCl. These results suggest that Γ_{XeCl^*} for Cl_2 with Xe(7p) atoms is actually ~0.7. The relative Γ_{XeCl^*} values for CCl_4 seem small, and they would be even smaller if scaled to $\Gamma_{XeF^*} = 1$ with NF_3 as a reference. The Γ_{XeCl^*} should be adjusted for $XeCl^*$ emission below 220 nm,[16] but this will add only ~10−15% to the values in Table 6 for Cl_2 and CCl_4, which are the only reagents in this list with high $\langle f_V(XeCl)\rangle$.[7] This adjustment would apply to both Xe(6p′) and Xe(7p) reactions, so the difference in Γ_{XeCl^*} values would still exist. The reaction of K(n=9) with CCl_4 has an ion-pair formation cross section[15f] similar to SF_6. Since EA(Cl_2) and EA(CCl_4) > EA(SF_6) and since Cl_2^- and CCl_4^- are dissociative,[39] perhaps some of the CCl_4^- and Cl_2^- ions eject $Cl^- + Xe^+$ ion-pairs from the Coulomb field in Xe(7p) reactions.

4. Models for Reactions with Halogen-Containing Molecules. The reagents can be divided into three group: (1) rare gases and CF_4, (ii) molecular reagents with large negative electron affinities (H_2, CO, CH_4, CH_3F, etc.), and (iii) halogen-containing molecules that attach electrons and have EA values ≥ −0.8 eV. The mechanisms for these three classes are (i) inter- and intramultiplet relaxation of Xe* via diabatic curve crossing[36] and/or Demkov coupling of parallel entrance and exit channel potentials,[17] (ii) excitation transfer to a high density of electronic states of the reagent, and (iii) electron transfer in the vicinity of the crossing of the diabatic covalent and ion-pair potentials in the entrance channel (and/or direct interaction of RX and the Rydberg electron). The quenching cross sections generally increase in the order listed, although exceptions exist, especially He and Ne collisions with certain Xe* levels that involve Demkov coupling.[17] We will focus on group (iii) and attempt to gain some insight regarding the very large cross sections.

The cross sections for electron attachment from Xe* or K* atoms with very high principal quantum numbers ($n \geq 20$) can be explained by the "essentially free electron" model, in which the collision of the projectile with the Rydberg atom is treated as an interaction with a free electron; for example, the cross sections for free electrons interacting with the reagent are the key factor in determining the quenching cross section.[15] For intermediate values of n, the fraction of collisions that can overcome the electrostatic attraction and form free ions must be considered; however, the interaction still was formulated as between the projectile and the electron rather than with the whole atom.[15e] The effective H-like principal quantum number for Cs(7p^{2}P$_{1/2}$) is $n^* = 3.374$, which corresponds to an average electron radius of ~9 Å, and the physical size for a Xe(7p) atom should be similar. This physical cross section of 250 Å^2 is similar to the quenching cross sections for H_2, CO, etc. The possibility that the CCl_4 and Cl_2 collisions may give some ion-pair product suggests that viewing the reaction as a coupling between the diabatic potential surfaces defined by R(Xe−XR) and r(R−X) may not be sufficient. To examine this question, we will focus on reactions with HCl, CF_2Cl_2, CCl_4, and Cl_2 because of the availability of calculations[8] for the diabatic coupling model for Xe(6p,6p′,7p) atoms with Cl_2, because of the molecular beam studies[13] of Na(3p,4d,5s) states with HCl and Cl_2 and because of predictions of how quenching cross sections should depend on EA(RX).

The ionization energies of Na(5s^{2}S$_{1/2}$) and Na(3p^{2}P$_{3/2}$) atoms are 1.02 and 3.03 eV, which are close to the ionization energies of the Xe(7p and 6p) states, respectively. The predicted reactive cross sections (for EA(HCl) = −0.815 eV)[40] from the harpoon model for NaCl formation from Na(5s) and Na(3p) with HCl are 192 and 47 Å^2, respectively.[13a] The experimental cross sections do increase with electronic excitation from ~0.06 Å for the Na(3s^{2}S$_{1/2}$) ground state to 6.5 and 27 Å^2 for Na(3p) and Na(5s), respectively. Nevertheless, the experimental cross sections (for $E_T = 5.6$ kcal mol^{-1}) are much smaller than the predictions of the model. Furthermore, NaCl is scattered mainly in the backward hemisphere, as consistent with the requirement of small impact parameter collisions with an orientation of the Cl end of HCl pointing toward the incoming Na atom. In contrast, the total cross sections ($\Gamma_{XeCl^*} \geq 0.5$) for Xe(7p) and Xe(6p) atoms are 800 and 170 Å^2, which is far *larger* than predictions from the harpoon model. We believe that this is evidence for direct interaction between the Rydberg electron of Xe(6p′,7p) atoms and the HCl molecule. The electron attachment cross section for HCl(v=0) has a maximum at 0.85 eV,[40] which is close to the kinetic energy of the Rydberg electron in Xe(7p) atoms.

The increase in Γ_{XeCl^*} from 0.02, 0.14, to ~1.0 for the reaction of CF_2Cl_2 with Xe(6s), Xe(6p), and Xe(7p) atoms is remarkable[6d] and illustrates how reactive quenching becomes more important than excitation transfer for polyatomic molecules as the Xe* electronic energy is increased. The EA$_v$(CF_2Cl_2) is not well established,[41] but it is about −0.1 eV. The diabatic curve-crossing distance becomes more favorable with electronic excitation, but the quenching cross section of Xe(7p) atoms by CCl_2F_2 is larger than predicted by the harpoon model. Dichlorodifluoromethane has a large electron attachment cross section for electrons with 0.6 eV of energy,[42] and direct interaction with the Rydberg electron seems a preferable explanation for quenching rather than a diabatic curve-crossing model. The smaller cross sections for Xe(6p′) vs Xe(7p) atoms with CF_2Cl_2 or with HCl cannot be explained as a preference for electron transfer at R_{X2} vs R_{X1}, because the XeCl(D) yields are small from the Xe(6p′) reaction. A simpler explanation for the reduced cross section, relative to Xe(7p) atoms, is the smaller electron attachment cross section for the higher kinetic energy of the Rydberg electron in Xe(6p′) atoms.

The description for NF_3 is similar to CF_2Cl_2, except that the Γ_{XeF^*} is sizeable even for Xe(6s) atoms, although the rate constant is small and $\langle f_V(XeF)\rangle$ is modest.[7] The larger Γ_{XeX^*}, relative to Γ_{XeCl^*} from CF_2Cl_2, for Xe(6s) atom reactions probably is related to the small probability for excitation transfer due to the sparse density of electronic states in NF_3,[12] even though the coupling to $V(Xe^+;NF_3^-)$ is at short range because EA(NF_3) is small.[43]

The diabatic curve-crossing model developed by Bruce et al. could explain the cross sections for Xe(6p′) and Xe(7p) atoms with CCl_4 by adjustment of the H_{12} matrix element, and the effective two-body potential[44] of CCl_4^-, including EA(CCl_4). On the basis of the data for K(n=9) + CCl_4,[15g] the free-electron scattering model also could explain the Xe(6p′,7p) quenching mechanism. The electron attachment cross section of CCl_4 has a maximum for zero energy electrons, declines with electron energy, and then subsequently increases to a second maximum at ~0.8 eV.[42,44]

The interaction potentials of Na(3s) and Na(3p) atoms with Cl_2 resemble those for Xe(6s) and Xe(6p) atoms, respectively, in terms of the R_{X1} values. The thermal cross sections for Na(3s) and Xe(6s) atoms are both consistent with the orbiting limit for the lower adiabatic potential. For EA$_v$(Cl_2) = 1.0 eV,[45] the cross sections of both Na(3p) and Xe(6p) are almost exactly in accord with the simple harpoon result, R_{X1}^2. The more complete model of Bruce et al.,[8] which includes the dependence of the interaction probability on r(Cl_2), gives the same cross section for Xe(6p) atoms, because the electron transfer prob-

ability is 1.0 for impact parameters $\leq R_{X1}$. The reactive scattering (forward hemisphere) and energy disposal (large $\langle f_V(NaCl)\rangle$ and small $\langle f_T(NaCl)\rangle$)[13b] are in accord with the large reactive cross section and repulsive nature of Cl_2^-; the energy disposal pattern to XeCl* is similar.[7] The Xe(7p) reaction presents an interesting test for the curve-crossing model. The nominal R_{X1} is very large (100 Å) for $EA_v(Cl_2) = 1.0$ eV. According to the standard parameters used to calculate H_{12}, the transfer probability would be very low and the Xe(7p) cross sections would be small. This is a commonly encountered problem for electronically excited atoms.[14c] Bruce et al.[8] circumvented this problem by extending the range of H_{12} to larger R and by including the vibrational motion of the $r(Cl_2)$ coordinate in their model, and they obtained a good fit to the reactive cross sections for Xe(7p) atoms. According to their calculations for Xe(7p[5/2]$_2$), the most probable distance for electron transfer is 10−20 Å; the coupling for this range of R is facilitated by the sensitive dependence of the electron affinity on the Cl_2 vibrational coordinate; that is, the EA_v decreases as $r(Cl_2)$ reaches the inner turning point. Since H_{12} rapidly increases with decreasing R, the Franck−Condon-allowed transitions at small $r(Cl_2)$ moved the effective coupling distance from 100 to 20 Å. An interesting consequence of Bruce's model is that the effective ranges for the outer and inner crossings are much closer than implied by R_{X1} and R_{X2} distances at $r_e(Cl_2)$. The success of Brue's model is *very* dependent on the shape of the Cl_2^- potential for small r. For most molecules insufficient information about RX^- exists to test the model. The free-electron scattering model provides an alternative explanation for the quenching of Xe(7p and 6p′) atoms by Cl_2; the close proximity of $V(Xe^*;Cl_2)$ and $V(Xe^+;Cl_2^-)$ at long range aids this model. Since interaction between Cl_2 and the Xe^+ ion-core also can occur, the electron scattering model provides a direct way to change the ion-core state for the Xe(6p′) reaction. An effort to incorporate the best aspects of both models into a unified description for reactions of intermediate level Rydberg states would be worthwhile.

Conclusions

Two-photon laser excitation of Xe has been used to study the relaxation and quenching of three states in the Xe(6p′ and 7p) manifolds by rare gases and by various molecules. The relative two-photon cross sections for states in the Xe(6p,6p′,7p) manifolds were compared and found to be of similar magnitude. Since numerous other Xe* states exist below 11 eV with zero concentration, amplified stimulated emission (ASE) occurs from the laser excited level, unless special precautions are taken. The ASE emission was characterized, and then experimental conditions were developed that permitted state-resolved kinetics to be studied without ASE emission. With reference to other published work, the decay constants of the Xe(6p′[3/2]$_2$, 7p[3/2]$_2$, and 7p[5/2]$_2$) states in He, Ne, and Ar can be interpreted in terms of state-to-state processes. The Xe* product states with small energy defects are favored for He and Ne collisions. The Xe(7p[1/2]$_1$) level, the lowest state in the 7p manifold, serves as a bottleneck to the transfer of Xe* concentration from the 7p, 6p′, and 6d manifolds to lower energy Xe* states in He or Ne bath gas. The product distributions from collisions with Ar and Xe tend to be broad, and Xe* product states with large energy defects are possible. In contrast, the deactivation of Xe(6p′,7p) atoms by Kr mainly gives Kr(5s,5s′) atoms as products, as first noted by Keto and co-workers.[3c]

The Xe(7p) and Xe(6p′) states have nearly the same energy, but formally different Xe^+ ion-core states. Experiments with CCl_4, CCl_2F_2, HCl, Cl_2, and NF_3 showed that the $Xe^+(^2P_{1/2})$ core is not conserved in the reactive quenching of Xe(6p′) atoms; that is, the Xe(6p′) and Xe(7p) atoms both gave mainly XeCl(B,C) and XeF(B,C) and not XeCl(D) and XeF(D). The simplest explanation for the lack of $Xe^+(^2P_{1/2})$ core conservation is the intrinsically mixed nature of the Xe^+ ion-core states for Xe(7p) and Xe(6p′) atoms. Another explanation could be the three-body nature of the interaction involving the Xe^+ core, the Rydberg electron, and the reagent molecule.

The quenching rate constants of Xe(6p′ and 7p) atoms by molecules are very large, with thermal cross sections ranging from 200 to 1500 Å^2. The rate constants for the Xe(7p) atoms for the same reagent tend to be ∼50% larger than those for Xe(6p′) atoms. Except for CF_4, which gives Xe* inter- and intramultiplet relaxation, molecules quench by excitation transfer or by electron transfer (chemical reaction). The very large cross section and high branching fraction for XeCl(B,C) formation by HCl suggest that the mechanism involves direct interaction of the reagent molecule with the Rydberg electron. The electron scattering and/or attachment cross sections of the halogen-containing molecules may offer better insight into the formulation of a quenching model[46] for Xe(6p′,7p) atoms than does the harpoon mechanism based on interaction of diabatic potential curves. Although the number of examples are limited, the data suggest that the dipole moment of the reagent molecule may have an influence on the quenching cross sections.

Acknowledgment. This work was supported by the National Science Foundation CHE-9402612. We wish to thank Drs. M. Bruce and J. Keto for extensive correspondence about results from their computations given in ref 8. The plots of calculated reaction probability for Xe(7p[5/2]$_2$) atoms with Cl_2, which they provided, were very helpful in providing an understanding of their model.

Supporting Information Available: Two-photon matrix elements for transitions to 6p, 6p′, and 7p states of Xe (2 pages). Ordering information is given on any current masthead page.

References and Notes

(1) (a) Ku, J. K.; Setser, D. W. *J. Chem. Phys.* **1986**, *84*, 4304. (b) Xu, J.; Setser, D. W. *J. Chem. Phys.* **1990**, *92*, 4191; **1991**, *94*, 4243.

(2) (a) Inoue, G.; Ku, J. K.; Setser, D. W. *J. Chem. Phys.* **1984**, *81*, 5706. (b) Horiguchi, H.; Chang, R. S. F.; Setser, D. W. *J. Chem. Phys.* **1981**, *75*, 1207.

(3) (a) Bruce, M. R.; Layne, W. B.; Whitehead, C. A.; Keto, J. W. *J. Chem. Phys.* **1990**, *92*, 2917. (b) Bowering, N.; Bruce, M. R.; Keto, J. W. *J. Chem. Phys.* **1986**, *84*, 709, 715. (c) Whitehead, C. A.; Pournasr, H.; Bruce, M. R.; Cai, H.; Kohel, J.; Layne, W. B.; Keto, J. W. *J. Chem. Phys.* **1995**, *102*, 1965. (d) Raymond, T. D.; Böwering, N.; Kuo, C.-Y.; Keto, J. W. *Phys. Rev. A.* **1984**, *29*, 721.

(4) (a) Allen, L.; Jones, D. G.; Schofield, D. G. *J. Opt. Soc. Am.* **1969**, *59*, 342. (b) McGee, T. J.; Burris, J.; Heaps, W. S.; Miller, G.; McIlrath, T. J. *J. Opt. Soc. Am.* **1985**, *B2*, 414.

(5) (a) Alford, W. J. *J. Chem. Phys.* **1992**, *96*, 4330. This reference summarizes the relaxation rate constants for Xe(6p) atoms in rare gases. (b) Museur, L.; Kanaev, A. V.; Zheng, W. Q.; Castex, M. C. *J. Chem. Phys.* **1994**, *101*, 10548. This reference describes the one-photon excitation of the Xe(5d[1/2]$_1$) level.

(6) (a) Ku, J. K.; Setser, D. W. *Appl. Phys. Lett.* **1986**, *48*, 689. (b) Setser, D. W.; Ku, J. K. In *Photochemistry and Photophysics above 6 eV*; Lahman, F., Ed.; Elsevier: Amsterdam, 1985. (c) Xu, J.; Setser, D. W.; Ku, J. K. *Chem. Phys. Lett.* **1986**, *132*, 427. (d) Slagle, A.; Xu, J.; Setser, D. W.; Ferrero, J. C. *Chem. Phys. Lett.* **1987**, *137*, 63.

(7) Nelson, T. O.; Richmann, M.; Setser, D. W. *J. Phys. Chem.* **1995**, *99*, 7482.

(8) (a) Bruce, M. R.; Layne, W. B.; Meyer, E.; Keto, J. W. *J. Chem. Phys.* **1990**, *92*, 420. (b) Bruce, M. R.; Layne, W. B.; Keto, J. W. *J. Chem. Phys.* **1990**, *92*, 428. (c) Keto, J. W.; Layne, W. B.; Bruce, M. R. In *Gas Phase Reactions of Metallic Atoms*; Fontijn, A., Ed.; Elsevier: Amsterdam, 1992.

(9) (a) Sadeghi, N.; Cheaib, M.; Setser, D. W. *J. Chem. Phys.* **1989**, *90*, 219. (b) Sobczynksi, R.; Beaman, R.; Setser, D. W.; Sadeghi, N. *Chem.*

Phys. Lett. **1989**, *154*, 349. (c) Zhong, D. P.; Setser, D. W. *J. Chem. Phys.*, to be submitted.

(10) (a) Tsuji, M.; Muraoka, T.; Kouno, H.; Nishimura, Y. *J. Chem. Phys.* **1992**, *97*, 1079. (b) Tsuji, M.; Furusawa, M.; Kouno, H.; Nishimura, Y. *J. Chem. Phys.* **1991**, *94*, 4291. (c) Tsuji, M.; Furusawa, M.; Nishimura, V. *J. Chem. Phys.* **1990**, *92*, 6502. (d) Tsuji, M.; Ide, M.; Muraoka, T.; Nishimura, Y. *J. Chem. Phys.* **1993**, *99*, 1710.

(11) Kvaran, A.; Ludviksson, A.; Hartree, W. S.; Simons, J. P. *Chem. Phys. Lett.* **1987**, *137*, 209.

(12) Chen, X.; Setser, D. W. *J. Phys. Chem.* **1991**, *129*, 82.

(13) (a) Weiss, P. S.; Mestdagh, J. M.; Covinsky, M. H.; Balko, B. A.; Lee, Y. T. *Chem. Phys.* **1988**, *126*, 93. (b) Weiss, P. S.; Mestdagh, J. M.; Schmidt, H.; Covinsky, M. H.; Lee, Y. T. *J. Phys. Chem.* **1991**, *95*, 3005. (c) Paillard, D.; Mestdagh, J. M.; Cuvellier, J.; de Pujo, P.; Berlande, J. *J. Chem. Phys.* **1987**, *87*, 2084; **1988**, *88*, 2398; **1989**, *91*, 6866. This set of papers describes electronically excited alkali metal atoms interacting with O_2.

(14) (a) Hertel, I. V. Progress in Electronic-to-Vibrational Energy Transfer. *Adv. Chem. Phys.* **1982**, *50*, 475; **1981**, *45*, 341. (b) Campbell, E. E. B.; Schmidt, H.; Hertel, I. V. Symmetry and Angular Momentum in Collisions with Laser-Excited Polarized Atoms. *Adv. Chem. Phys.* **1988**, *72*, 37. (c) Berson, R. In *Alkali Halide Vapors*; Davidovits, P., McFadden, D. L., Eds.; Academic: New York, 1979.

(15) (a) Astruc, J. P.; Desfrancois, C.; Barbe, R.; Schermann, J. P. *J. Chem. Phys.* **1988**, *88*, 106. (b) Hickman, A. P. *Phys. Rev. A* **1981**, *23*, 87. (c) Olson, R. E. *Phys. Rev. A* **1977**, *15*, 631. (d) Gounand, F.; Berlande, J. in *Rydberg States of Atoms and Molecules*; Stebbings, R. F., Dunning, F. B., Eds.; Cambridge University Press: Cambridge, 1983. (e) Kellert, F. G.; Smith, K. A.; Rundel, R. D.; Dunning, F. B.; Stebbings, R. F. *J. Phys. Chem.* **1980**, *72*, 3179, and other papers in this series. (f) Zollars, B. G.; Walter, C. W.; Lu, F.; Johnson, C. B.; Smith, K. A.; Dunning, F. B. *J. Chem. Phys.* **1986**, *84*, 5589.

(16) Zhong, D.; Setser, D. W. *Chem. Phys. Lett.* **1993**, 207, 555.

(17) Zikratov, G.; Setser, D. W. *J. Chem. Phys.* **1996**, *104*, 2243.

(18) (a) Rankin, M. B.; Davis, J. P.; Giranda, C.; Bobb, L. G. *Opt. Commun.* **1989**, *70*, 345. (b) Miller, J. C. *Phys. Rev. A* **1989**, *40*, 6969.

(19) (a) Miyazaki, K.; Sakai, H.; Sato, T. *Appl. Opt.* **1989**, *28*, 699. (b) Hepburn, J. W. *Isr. J. Chem.* **1984**, *24*, 273. (c) Hilbig, R.; Wallenstein, *IEEE J. Quantum Electron.* **1983**, *QE-19*, 194.

(20) (a) Aymar, M.; Coulombe, M. *At. Data Nucl. Data Tables* **1978**, *21*, 538. (b) The relative intensities from the 473.4 and 452.5 lines were recorded from laser excitation at low laser energy (non-ASE conditions) and from a laser-induced plasma to be 2.3 in favor of the 473.4 nm line. This ratio agrees with the ratio in ref 2b, which disagrees with the calculated ratio (1.0). The oscillator strengths given by ref 20c generally favor the branching ratios of ref 2b. (c) Sabbagh, J.; Sadeghi, N. *J. Quantum Spectrosc. Radiat. Transfer* **1977**, *17*, 297. (d) Chang, W. F.; Cooper, G.; Guo, X.; Burton, G. R.; Brion, C. E. *Phys. Rev. A* **1992**, *46*, 149.

(21) Lu, Y.; Morioka, Y.; Matsui, T.; Tanaka, T.; Yoshi, H.; Hall, R. I.; Hayaishi, T.; Ito, K. *J. Chem. Phys.* **1995**, *102*, 1553.

(22) Moller, T.; Beland, M.; Zimmerer, G. *Chem. Phys. Lett.* **1987**, *136*, 551.

(23) (a) Lipson, R. H. *Chem. Phys. Lett.* **1986**, *129*, 82. (b) Dabrowski, I.; Herzberg, G.; Lipson, R. H. *Mol. Phys.* **1988**, *63*, 289.

(24) Gürtler, P.; Kraas, M.; Tschentsher, T. *Europhys. Lett.* **1990**, *11*, 115.

(25) Petsalakis, I. D.; Theodorakopoulos, G.; Consta, S. *Mol. Phys.* **1992**, *75*, 805.

(26) Kawasaki, M.; Matsumi, Y.; Chattopadhyay, A.; Shafer, N.; Satyapal, S.; Tasaki, S.; Yi, W.; Bersohn, R. *J. Phys. Chem.* **1992**, *96*, 7010.

(27) Twist, J. R.; Paske, W. C.; Rhymes, T. O.; Haddard, G. H.; Golden, D. E. *J. Chem. Phys.* **1979**, *71*, 2345.

(28) Sadeghi, N.; Colomb, I.; Stoyanova, J.; Setser, D. W.; Zhong, D. *J. Chem. Phys.* **1995**, *102*, 2744.

(29) (a) Tsuji, M.; Yamaguchi, K.; Nishimura, Y. *Chem. Phys.* **1988**, *125*, 337. (b) Krumpelmann, T.; Ottinger, Ch. *Chem. Phys. Lett.* **1987**, *140*, 142. (c) Chow-Chin, L.; Krumpelmann, T.; Ottinger, Ch. *Chem. Phys. Lett.* **1989**, *157*, 60.

(30) (a) Neesev, S.; Voitik, M.; Langhoff, H. *J. Chem. Phys.* **1995**, *102*, 1639. (b) Johnson, D. E. *Chem. Phys. Lett.* **1995**, *238*, 71.

(31) (a) Rives, P.; Teyssier, J. L.; Galy, J.; Birot, A.; Brunet, H.; Asselman, H. *J. Chem. Phys.* **1995**, *102*, 1217. This reference gives a summary of the relaxation kinetics of XeCl(B,C) in a Xe/HCl mixture. The rate constant for B/C mixing increases for higher v' levels. (b) Yu, Y. C.; Wategaonkar, S. J.; Setser, D. W. *J. Chem Phys.* **1992**, *96*, 8914.

(32) Alekseev, V.; Setser, D. W. *J. Chem. Phys.* To be published.

(33) Gornik, W.; Kindt, S.; Matthias, E.; Schmidt, D. *J. Chem. Phys.* **1981**, *75*, 68.

(34) (a) Wijngaarden, W. A.; Li, J. *J. Quantum Spectrosc. Radiat. Transfer* **1994**, *52*, 555. According to this reference, the polarizabilities of Cs(6s), Cs(6p), Cs(7s), and Cs(7p) atoms are 58, 192, 914, and 4380 $Å^3$, respectively. Since the experimental polarizabilities of Xe(6s), 62.6 $Å^3$, and Cs(6s), 61.5 $Å^3$, atoms are similar,[34b] we have used the polarizabilities of the corresponding Cs* atom for the Xe* states. (b) Molof, R. B.; Schwartz, H. L.; Miller, T. M.; Bederson, B. *Phys. Rev.* **1974**, *A10*, 1131.

(35) (a) Liberman, S. *J. Phys.* **1969**, *30*, 53. (b) Coulombe, M. C.; Sinzelle, J. *J. Phys.* **1975**, *36*, 774.

(36) Hickman, A. P.; Huestis, D. L.; Saxon, R. P. *J. Chem. Phys.* **1992**, *96*, 2099.

(37) Hershberger, J. F.; Huh, Y. D.; McAndrew, J. J.; Cross, R. J.; Saunders, M. *J. Am. Chem. Soc.* **1988**, *110*, 1104.

(38) (a) Campbell, M. L.; Furio, N.; Dagdiagian, P. J. *Laser Chem.* **1986**, *6*, 391. (b) Verdasco, E.; Rabanos, V. S.; Gonzalez-Urena, A. *Laser Chem.* **1989**, *10*, 51.

(39) (a) Chen, E. C. M.; Shuie, L.-R.; D'sa, E. D.; Batten, C. F.; Wentworth, W. E. *J. Chem. Phys.* **1989**, *88*, 4711. (b) Orient, O. J.; Chutjian, A. *Phys. Rev. A.* **1986**, *34*, 1841. (c) Smith, D.; Adams, N. G.; Alge, E. *J. Phys. B.* **1984**, *17*, 461. (d) Datskos, P. G.; Carter, J. G.; Christophorou, L. G. *Chem. Phys. Lett.* **1995**, *239*, 38. (e) Weston, R. E., Jr. *J. Phys. Chem.* **1995**, *99*, 13150.

(40) Bardsky, J. N.; Wadehra, J. M. *J. Chem. Phys.* **1983**, *78*, 7227.

(41) Sobczynski, R.; Setser, D. W.; Slagle, A. R. *J. Chem. Phys.* **1990**, *92*, 1132.

(42) (a) Jones, R. K. *J. Chem. Phys.* **1986**, *84*, 813. (b) McCorkle, D. L.; Christodoulides, A. A.; Christophorou, L. G.; Szamrez, I. *J. Chem. Phys.* **1980**, *72*, 4049.

(43) Harland, P. W.; Franklin, J. L. *J. Chem. Phys.* **1974**, *61*, 1621.

(44) (a) Roszak, S.; Kaufman, J. J.; Kosk; W. S.; Vijayakumar, M.; Balasubramanian, K. *J. Chem. Phys.* **1994**, *101*, 2978. (b) Guerra, M.; Jones, D.; Distefano, G.; Scagmolari, F.; Modelli, A. *J. Chem. Phys.* **1991**, *94*. 484. (c) Olthoff, J. K.; Moore, J. H.; Tossell, J. A. *J. Chem. Phys.* **1986**, *85*, 249.

(45) Nelson, T. D.; Setser, D. W.; Qin, J. *J. Phys. Chem.* **1993**, *97*, 2585.

(46) Schermann, J. P.; Astruc, J. P.; Desfrancois, C.; Barbé, R. In *Photoinduced Electron Transfer*; Fox, M. A., Chanon, M., Eds.; Elsevier: Amsterdam, 1988; Part A.

JP952402C